



University of Maribor

Faculty of Energy Technology

# Journal of ENERGY TECHNOLOGY



Volume 15 / Issue 1

JUNE 2022

[www.fe.um.si/jet.html](http://www.fe.um.si/jet.html)



# Journal of ENERGY TECHNOLOGY



**VOLUME 15 / Issue 1**

Revija Journal of Energy Technology (JET) je indeksirana v bazah INSPEC® in Proquest's Technology Research Database.

The Journal of Energy Technology (JET) is indexed and abstracted in database INSPEC® and Proquest's Technology Research Database.



# JOURNAL OF ENERGY TECHNOLOGY

## **Ustanovitelj / FOUNDER**

Fakulteta za energetiko, UNIVERZA V MARIBORU /  
FACULTY OF ENERGY TECHNOLOGY, UNIVERSITY OF MARIBOR

## **Izdajatelj / PUBLISHER**

Fakulteta za energetiko, UNIVERZA V MARIBORU /  
FACULTY OF ENERGY TECHNOLOGY, UNIVERSITY OF MARIBOR

## **Glavni in odgovorni urednik / EDITOR-IN-CHIEF**

Jurij AVSEC

## **Souredniki / CO-EDITORS**

Bruno CVIKL  
Miralem HADŽISELIMOVIĆ  
Gorazd HREN  
Zdravko PRAUNSEIS  
Sebastijan SEME  
Bojan ŠTUMBERGER  
Janez USENIK  
Peter VIRTič  
Ivan ŽAGAR

## **Uredniško izdajateljski svet / PUBLISHING & EDITORIAL COUNCIL**

**Dr. Anton BERGANT,**  
Litostroj Power d.d., Slovenia

**Prof. dr. Marinko BARUKČIĆ,**  
Josip Juraj Strossmayer University of Osijek, Croatia

**Prof. dr. Goga CVETKOVSKI,**  
Ss. Cyril and Methodius University in Skopje, Macedonia

**Prof. dr. Nenad CVETKOVIĆ,**  
University of Nis, Serbia

**Prof. ddr. Denis ĐONLAGIĆ,**  
University of Maribor, Slovenia

**Doc. dr. Brigita FERČEC,**  
University of Maribor, Slovenia

**Prof. dr. Željko HEDERIĆ,**  
Josip Juraj Strossmayer University of Osijek, Croatia

**Prof. dr. Marko JESENIK,**  
University of Maribor, Slovenia

**Izr. prof. dr. Ivan Aleksander KODELI,**  
Jožef Stefan Institute, Slovenia

**Izr. prof. dr. Rebeka KOVAČIČ LUKMAN,**  
University of Maribor, Slovenia

**Prof. dr. Milan MARČIČ,**  
University of Maribor, Slovenia

**Prof. dr. Igor MEDVED,**  
Slovak University of Technology in Bratislava, Slovakia

**Izr. prof. dr. Matej MENCINGER,**  
University of Maribor, Slovenia

**Prof. dr. Greg NATERER,**  
Memorial University of Newfoundland, Canada

**Prof. dr. Enrico NOBILE,**  
University of Trieste, Italia

**Prof. dr. Urška LAVREŇIČ ŠTANGAR,**  
University of Ljubljana, Slovenia

**Izr. prof. dr. Luka SNOJ,**  
Jožef Stefan Institute, Slovenia

**Prof. Simon ŠPACAPAN,**  
University of Maribor, Slovenia

**Prof. dr. Gorazd ŠTUMBERGER,**  
University of Maribor, Slovenia

**Prof. dr. Anton TRNIK,**  
Constantine the Philosopher University in Nitra, Slovakia

**Prof. dr. Zdravko VIRAG,**  
University of Zagreb, Croatia

**Prof. dr. Mykhailo ZAGIRNYAK,**  
Kremenchuk Mykhailo Ostrohradskyi National University, Ukraine

**Prof. dr. Marija ŽIVIĆ,**  
Josip Juraj Strossmayer University of Osijek, Croatia

**Tehnični urednik / TECHNICAL EDITOR**

Sonja Novak

**Tehnična podpora / TECHNICAL SUPPORT**

Tamara BREČKO BOGOVČIČ

**Izhajanje revije / PUBLISHING**

Revija izhaja štirikrat letno v nakladi 100 izvodov. Članki so dostopni na spletni strani revije – <https://www.fe.um.si/jet.html> / The journal is published four times a year. Articles are available at the journal's home page – [www.fe.um.si/en/jet.html](http://www.fe.um.si/en/jet.html).

Cena posameznega izvoda revije (brez DDV) / Price per issue (VAT not included in price): 50,00 EUR  
Informacije o naročninah: <https://www.fe.um.si/naro%C4%8Dnine.html> / Subscription information: <https://www.fe.um.si/en/subscriptions.html>

**Lektoriranje / LANGUAGE EDITING**

TAIA INT d.o.o.

**Oblikovanje in tisk / DESIGN AND PRINT**

Tiskarna Koštomaj d.o.o.

**Naslovna fotografija / COVER PHOTOGRAPH**

Jurij AVSEC

**Oblikovanje znaka revije / JOURNAL AND LOGO DESIGN**

Andrej PREDIN

**Ustanovni urednik / FOUNDING EDITOR**

Andrej PREDIN

---

Izdajanje revije JET finančno podpira Javna agencija za raziskovalno dejavnost Republike Slovenije iz sredstev državnega proračuna iz naslova razpisa za sofinanciranje domačih znanstvenih periodičnih publikacij / The Journal of Energy Technology is co-financed by the Slovenian Research Agency.

## ***Spoštovani bralci revije Journal of energy technology (JET)***

Razumno in učinkovito upravljanje z energijo oz. energetika je izjemnega pomena za doseg gospodarske blaginje vsake države. Žal se je v zgodovini ogromno vojn odvijalo prav zaradi energetike oz. dostopa do energije. Videti je, da je poglaviti vzrok vojne v Ukrajini prav zaradi nadzora nad energetske viri. Tudi Slovenija je na razpotju, kako v prihodnosti upravljati z energijo. V Sloveniji obstajata največja energetska bazena v Krškem in v Velenju. V Krškem se v bližnji prihodnosti pričakuje graditev nove jedrske elektrarne, v Velenju pa se prav tako obetajo spremembe, ki se bodo zgodile po eri premoga. Vsekakor je izjemnega pomena ohraniti vse energetske lokacije v njihovi funkciji.

V bližnji prihodnosti je treba prav tako vložiti napore in raziskovalna sredstva v projekte za izkoriščanje obnovljivih virov v čim večji možni meri. Slovenija kot zelena dežela lahko izkoristi potencial obnovljivih virov za doseg čim večje energetske samooskrbnosti. Želja po samooskrbnosti je še toliko pomembnejša, saj se v bližnji prihodnosti obetajo velike podražitve vseh vrst energij. Veliko si obetamo tudi od masovne uporabe vodikovih tehnologij.

V Velenju bo 14. junija mednarodna konferenca EnRe 2022 prav z namenom izmenjave mnenj. Na njej bodo vabljeni predavatelji in raziskovalci predstavili svoje poglede na razvoj energetike v Sloveniji in v svetu. Zato vabim vse, ki jih energetika zanima, da pridejo v Velenje na konferenco Enre.

Jurij AVSEC  
odgovorni urednik revije JET



## ***Dear Readers of the Journal of Energy Technology (JET)***

Reasonable and efficient energy management or energy engineering is extremely important for all countries in terms of achieving economic prosperity. Unfortunately, throughout history, many wars have taken place precisely because of energy or access to energy, and it seems that the main cause of the war in Ukraine is also due to the desire to have control over energy resources. Slovenia is at a crossroads in terms of how to manage energy in the future. The country's largest energy basins are in Krško and Velenje. Construction of a new nuclear power plant is expected in the near future in Krško, while in Velenje, changes are expected that will take place after the coal era. It is certainly extremely important to maintain the function of all these energy locations.

In the near future, there needs to be significant endeavours and investments in renewable energy projects. As a green country, Slovenia can use the potential of renewable resources to achieve maximum energy self-sufficiency. The desire for self-sufficiency is even more important, as large increases in all types of energy are expected in the near future. The mass use of hydrogen technologies also holds great promise.

The international EnRe 2022 conference will take place in Velenje on 14 June 2022. The aim of the conference is to offer participants the opportunity to exchange views. Guest lecturers and researchers will provide their views on the development of energy in Slovenia and elsewhere in the world. Therefore, I invite all those who are interested in energy to come to Velenje for the EnRe conference.

Jurij AVSEC  
Editor-in-chief of JET

# ***Table of Contents / Kazalo***

## **Method of the best available technology and low carbon future of a combined heat and power plant**

Metoda najboljše razpoložljive tehnologije in nizkoogljična prihodnost toplarniškega postrojenja

**Dušan Strušnik, Marko Agrež . . . . . 11**

## **The impact of unbalanced power supply on load currents in transient and steady-state operation**

Vpliv nesimetričnih napajalnih napetosti na toke bremen med ustaljenim obratovanjem in med prehodnimi pojavi

**Nina Štumberger, Matej Pintarič, Gorazd Štumberger . . . . . 23**

## **Reducing carbon footprint on OEM supply chain caused by inadequate interpretation of X-ray results of hidden defects in ductile iron castings**

Zmanjšanje ogljičnega odtisa v dobavni verigi OEM-ov zaradi neustrezne interpretacije rezultatov RTG skritih napak v nodularni litini

**Tadej Pavlin, Iztok Brinovar, Bojan Stergar, Zdravko Praunseis . . . . . 51**

## **Hamiltonicity of certain cartesian products of graphs**

Hamiltonskost kartezičnega produkta grafov

**Tjaša Paj Erker . . . . . 67**

**Instructions for authors . . . . . 73**

# METHOD OF THE BEST AVAILABLE TECHNOLOGY AND LOW CARBON FUTURE OF A COMBINED HEAT AND POWER PLANT

## METODA NAJBOLJŠE RAZPOLOŽLJIVE TEHNOLOGIJE IN NIZKOOGLJIČNA PRIHODNOST TOPLARNIŠKEGA POSTROJENJA

Dušan Strušnik<sup>1✉</sup>, Marko Agrež<sup>1</sup>

**Keywords:** alternative facilities, best available technology, combined plant, heat recovery, hydrogen, low-carbon, methanisation, natural gas, steam recovery Abstract

### **Abstract**

The low-carbon development strategy and ecological awareness of a combined heat and power (*CHP*) plant is the key factor that enables further development of such systems. *CHP* plants are subject to rigid European ecological guidelines, which dictate the pace of development of global thermal power engineering. For this purpose, the European Union issued a special Directive for the promotion of heat and power cogeneration, and is established with the best available technology (*BAT*) method. Even though the production of electricity using carbon-free technologies is on the rise, the production of electricity by fossil fuel combustion cannot be avoided completely. The meaning of the operation of the *CHP* plant is reflected particularly in the provision of tertiary services to the electric power system, regulation of the network frequency, particularly in winter

<sup>✉</sup> Corresponding author: Dušan Strušnik, Energetika Ljubljana d.o.o., TE-TOL Unit, Toplarniška ulica 19, SI-1000 Ljubljana, Slovenia, Phone: +386 31 728 652, [dusan.strusnik@gmail.com](mailto:dusan.strusnik@gmail.com)

<sup>1</sup> Energetika Ljubljana d.o.o., TE-TOL Unit, Toplarniška ulica 19, SI-1000 Ljubljana, Slovenia

months, when electricity production using carbon-free technologies is limited. In *CHP* systems, the low-carbon future is linked intricately to high investment costs and these impacts the final price of energy. Using the *BAT* method, the article presents the advantages of energy production in a combined heat and power plant, an example of the restructuring of a larger *CHP* system into a low-carbon plant and guidelines for further development.

## **Povzetek**

Nizkoogljična razvojna strategija in ekološka ozaveščenost toplarniškega postrojenja sta ključna dejavnika, ki omogočata nadaljnji razvoj tovrstnih sistemov. Toplarniška postrojenja so podvržena strogim evropskim ekološkim smernicam, ki narekujejo tempo razvoja globalne termoenergetike. V ta namen je Evropska unija izdala posebno direktivo za spodbujanje proizvodnje toplote in električne energije v kogeneraciji, ki se ugotavlja z metodo najboljše razpoložljive tehnologije. Kljub temu da je proizvodnja električne energije s pomočjo brezogljičnih tehnologij v porastu, pa se proizvodnji električne energije s sežigom fosilnih goriv ne bo mogoče popolnoma izogniti. Pomen delovanja toplarniškega postrojenja se še zlasti izraža pri nudenju terciarnih storitev elektroenergetskemu sistemu, pri regulaciji frekvence omrežja, še zlasti v zimskih mesecih, ko je proizvodnja električne energije s pomočjo brez ogljičnih tehnologij okrnjena. V toplarniških sistemih je nizkoogljična prihodnost tesno povezana z velikimi investicijskimi stroški, ki vplivajo na končno ceno energije. S pomočjo metode najboljše razpoložljive tehnologije so v prispevku predstavljene prednosti proizvodnje energije v kogeneraciji, primer prestrukturiranja večjega toplarniškega sistema v nizkoogljično postrojenje ter smernice nadaljnjega razvoja.

## **1 INTRODUCTION**

The basic purpose of *CHP* systems is high-efficiency cogeneration of electricity. A *CHP* system is composed of a heat generator, a thermal engine and a heat sink. The heat generator serves for heat generation. A share of the generated thermal energy is converted by the thermal engine into mechanical work [1], and another share of the thermal energy may be used for industrial purposes in the form of industrial steam or for remote heating purposes [2]. The remaining part of unused heat is discharged into the environment. Unused heat refers to the heat which reduces the efficiency of the *CHP* plant [3]. In *CHP* systems where heat is generated by fossil fuel combustion, the largest share of such unused heat is exported to the environment through exhaust systems, and leaves combustion plants in the form of flue gases and through condensate systems. The advantages of energy production by means of *CHP* systems are expressed in the amount of heat discharged into the environment, because the minimisation of discharged heat increases the efficiency of such plant significantly. The simplest way of determining the suitability of a *CHP* plant is performed using the *BAT* method. What applies to *BAT* today, may be gone tomorrow. Using the *BAT* method, we have compared the co-generation of heat and power with separate production in alternative facilities [4]. Alternative facilities are facilities where electric and thermal energy are generated separately in separate facilities. Using alternative facilities, the *BAT* method, in addition to efficiency, also presents fuel savings. Because less fuel is used in *CHP* systems for the production of the same amount of energy than in separate facilities, the emissions of greenhouse gases are also correspondingly lower.

In addition to high-efficiency co-generation of energy, *CHP* systems are becoming increasingly more eco-friendly, because the adaptation to the best available technologies also contributes to the replacement of fuel types, thereby getting closer and closer to a carbon-free society and carbon neutrality [5]. This results in increased use of carbon-neutral fuels, such as biomass, biomass

fraction of waste, hydrogen, etc. In addition to carbon neutrality, special attention should also be directed to the reduction of emissions of other greenhouse and toxic gases, which are released in the process of the combustion of combustible substances. Reduction of greenhouse and toxic gases in combustion plants is only possible with precisely targeted development strategies, but it is largely connected to high investment costs. In Slovenian thermal power engineering, heat is largely generated by the combustion of coal, lignite, thermo-degradable waste and gas. Due to the high prices of emission coupons and related financial unsustainability, *CHP* systems are forced to transition to the use of carbon-neutral fuels and gasification of *CHP* systems. With the gasification of *CHP* systems, a share of the primary fuel or coal can be substituted by gas. The advantage of gas is expressed mainly in lower emissions of  $CO_2$  greenhouse gas, because it is largely composed of methane,  $CH_4$ , where hydrogen also undergoes combustion in addition to the carbon [6]. The advantage of the use of gas is also expressed in the production method, because, in addition to the utilisation of natural resources, in the process of methanisation gas can also be obtained by utilising energy surpluses, Power-to-Gas [7], and in a combination of biogas and hydrogen. Gas obtained in the process of methanisation can also be stored and used when energy demand increases. The European guidelines also provide for the construction of the European hydrogen pipeline, which would interconnect hydrogen producers, consumers and reservoirs. For this purpose, the European Union also established the European Clean Hydrogen Alliance [8], which indicates the first signs of the construction of hydrogen pipelines.

The article is structured so as to introduce the advantages of *CHP* systems initially in comparison to the generation of an equal amount of energy in separate alternative facilities using the *BAT* method. This is followed by the presentation of the steps of the low-carbon transformation of a large *CHP* plant and the guidelines for further development.

## 2 MODEL OF THE *BAT* METHOD OF ALTERNATIVE FACILITIES

The *BAT* method of alternative facilities refers to the European Directive 2004/8/ES [9] on the promotion of the production of heat and power in a co-generation process. The *BAT* method of alternative facilities compares the energy efficiency of a *CHP* system with the efficiency of facilities in separate production, or production of energy products in substitute facilities. The level of production efficiency is determined using the results of fuel savings. If heat and power production by means of the *CHP* system is more efficient than production in alternative facilities, the *CHP* system consumes less fuel, the system efficiency is improved, and the emissions of greenhouse gases and the toxicity of gases are lower. A schematic presentation of the model of the *BAT* method of alternative facilities is shown in Figure 1.

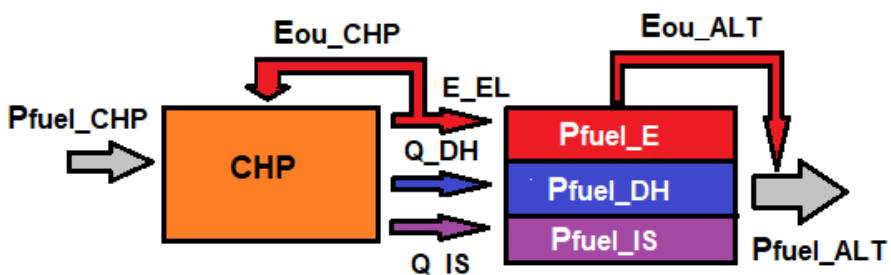


Figure 1: Schematic presentation of the model of the *BAT* method of alternative facilities

Figure 1 shows abbreviations, where  $P_{fuel\_CHP}$  is the fuel power for electricity and heat production of the *CHP* system,  $E_{EL}$  is the generated electric power,  $E_{out\_CHP}$  is the electric power of own use of the *CHP* system,  $Q_{DH}$  is the generated thermal power of remote heating,  $Q_{IS}$  is the generated thermal power of industrial steam,  $P_{fuel\_E}$  is the fuel power for generation of electric power by means of an alternative facility,  $P_{fuel\_DH}$  is the fuel power for the generation of thermal power of remote heating by means of an alternative facility,  $P_{fuel\_IS}$  is the fuel power for the generation of thermal power of industrial steam by means of an alternative facility,  $E_{ou\_ALT}$  is the total electric power of own use of alternative facilities, and  $P_{fuel\_ALT}$  is the total fuel power for the production of electric and thermal power of alternative facilities, where the generated electric and thermal power of the *CHP* system is equivalent to the electric and thermal power of the alternative facilities.

In our case, the *CHP* system consists of a combined cycle gas turbine (*CCGT*), composed of a gas turbine, steam generator and steam turbine. The analysis takes into account that, throughout the operation period, the *CCGT* steam turbine operates with a back-pressure at high efficiency. In an alternative facility, electric power is generated by means of a steam turbine in a pure condensation operation. The thermal power of remote heating in an alternative facility is generated by means of a hot water boiler. The thermal power of industrial steam in an alternative facility is generated by means of a steam boiler. Natural gas is used in the *CHP* system, as well as in substitute facilities. Fuel savings are calculated by means of the following equation [9]:

$$S_{fuel} = 1 - \left( \frac{1}{\frac{P_{fuel_E}}{P_{fuel_{CHP}}} + \frac{P_{fuel_{DH}}}{P_{fuel_{CHP}}} + \frac{P_{fuel_{IS}}}{P_{fuel_{CHP}}}} \right) \cdot 100 \quad (2.1)$$

where  $S_{fuel}$  are the fuel savings. The fuel power for the generation of electric power and thermal power of remote heating and technological steam of the *CHP* system is calculated by means of the following equation [10]:

$$P_{fuel_{CHP}} = LHV_{fuel} \cdot \dot{m}_{fuel} \quad (2.2)$$

where  $HHV_{fuel}$  is the higher heating value of natural gas and  $\dot{m}_{fuel}$  is the fuel mass flow. The calculation takes into account the lower calorific value of natural gas, which is 49,22 MJ/kg. Fuel power in alternative facilities is calculated by means of the following equations [9]:

$$P_{fuel_E} = \frac{E_{EL}}{\eta_E} \cdot 100 \quad (2.3)$$

$$P_{fuel_{DH}} = \frac{Q_{DH}}{\eta_{DH}} \cdot 100 \quad (2.4)$$

$$P_{fuel_{IS}} = \frac{Q_{IS}}{\eta_{IS}} \cdot 100 \quad (2.5)$$

where  $\eta_E$  is the efficiency of the alternative facility for generation of electric power,  $\eta_{DH}$  is the efficiency of the alternative facility for the generation of thermal power of remote heating, and  $\eta_{IS}$  is the efficiency of the alternative facility for the generation of thermal power of industrial steam. The total fuel power for the production of electric and thermal power of alternative facilities is calculated by means of the following equation:

$$P_{fuel_{ALT}} = P_{fuel_E} + P_{fuel_{DH}} + P_{fuel_{IP}} \quad (2.6)$$

## 2.1 Results of the BAT method of alternative facilities

The results of the *BAT* method of alternative facilities are structured so that they initially present the generated electric and thermal power and fuel power of the *CHP* system. This is followed by the presentation of fuel power for the operation of the alternative facilities. Fuel efficiency and savings are presented at the end. Figure 1 shows the fuel power required for the generation of electric and thermal power, depending on the *CHP* system load. At a 40% *CHP* system load the fuel power is 150 MW, while the *CHP* system generates 50 MW of electric power, 62 MW of thermal power of remote heating and 2 MW of thermal power of industrial steam. At a 100% *CHP* system load, the fuel power is 280 MW, while the *CHP* system generates 105 MW of electric power, 93 MW of thermal power of remote heating and 21 MW of thermal power of industrial steam.

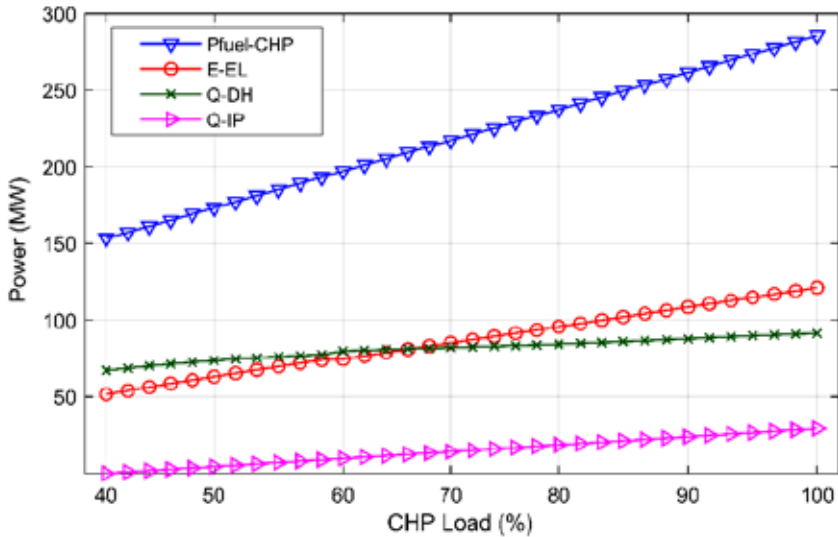


**Figure 2:** Fuel power, generated electric power, generated thermal power of remote heating and generated thermal power of industrial steam, depending on the *CHP* system load

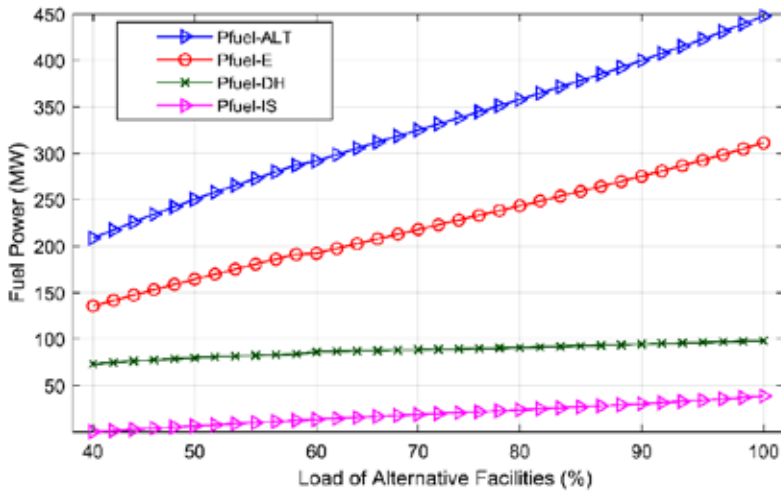


**Figure 3:** Fuel power for the operation of alternative facilities depending on the load

Figure 3 shows the fuel powers required for the operation of alternative facilities. At a 40% load of alternative facilities, fuel power for the generation of electric power is 140 MW, fuel power for the generation of thermal power of remote heating is 70 MW, fuel power for the generation of thermal power of industrial steam is 2.24 MW. At a 40% load of alternative facilities, total fuel power is 212.24 MW. At a 100% load of alternative facilities, fuel power for the generation of electric power is 307 MW, fuel power for the generation of thermal power of remote heating is 90 MW, fuel power for the generation of thermal power of industrial steam is 45 MW. At a 100% load of alternative facilities, total fuel power is 442 MW. Figure 4 shows the efficiency of the CHP system, total efficiency of alternative facilities and fuel savings in a cogeneration process.

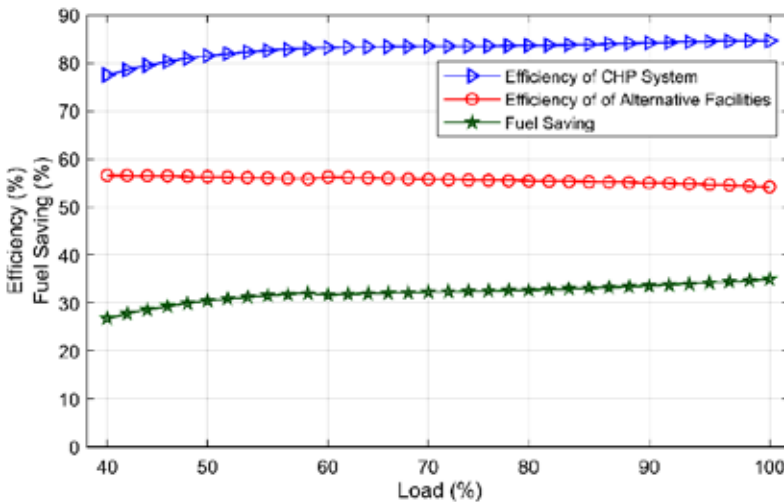


**Figure 4:** Efficiency of the CHP system, total efficiency of the alternative facilities and fuel savings of the CHP system



At a 40% load, the efficiency of the *CHP* system is 78%, and the total efficiency of alternative facilities is 58%. The fuel savings of the co-generation *CHP* production versus energy production by means of alternative facilities is 27%. At a 100% load, the efficiency of the *CHP* system is 87%, and the total efficiency of alternative facilities is 53%. The fuel savings of co-generation *CHP* production versus energy production by means of alternative facilities in this case amounts to 34%. By increasing the load the co-generation production efficiency by means of the *CHP* system increases, whereby the efficiency of production by means of alternative facilities decreases. Accordingly, increased load contributes to higher fuel savings. The cause of the reduced efficiency in an increased production load by means of alternative facilities is the increase in the dissipation of heat in the surroundings at pure condensation operation of a steam turbine or an alternative facility for the generation of electric power.

### **3 LOW-CARBON TRANSFORMATION OF A LARGE *CHP* SYSTEM AND GUIDELINES FOR FURTHER DEVELOPMENT**

In large *CHP* systems the combustion process with the purpose of increasing the enthalpy of a working medium is carried out by means of fossil fuel combustion. The type of fuel combusted is linked intricately to the chemical composition and corresponding greenhouse gas emissions. The low-carbon transformation of a large *CHP* system is linked intricately to the use of low-carbon or carbon-neutral fuels, such as biomass, biomass fraction of waste, hydrogen, etc. Replacement of the fuel type in *CHP* systems is linked intricately to high investment costs, because, in order to achieve high efficiency, it is required to opt for *BAT*. This raises the question as to what extent does it make sense to preserve the existing plant? However, replacing solid fuel with gas fuel, taking into account the high-efficiency *BAT*, results in the replacement of the entire *CHP* system. Figure 5 shows two *CHP* systems, specifically, Figure 5 a) shows the classic Rankine *CHP* system, and Figure 5 b) shows the combined Brayton-Rankine *CHP* high-efficiency gas-fired system.

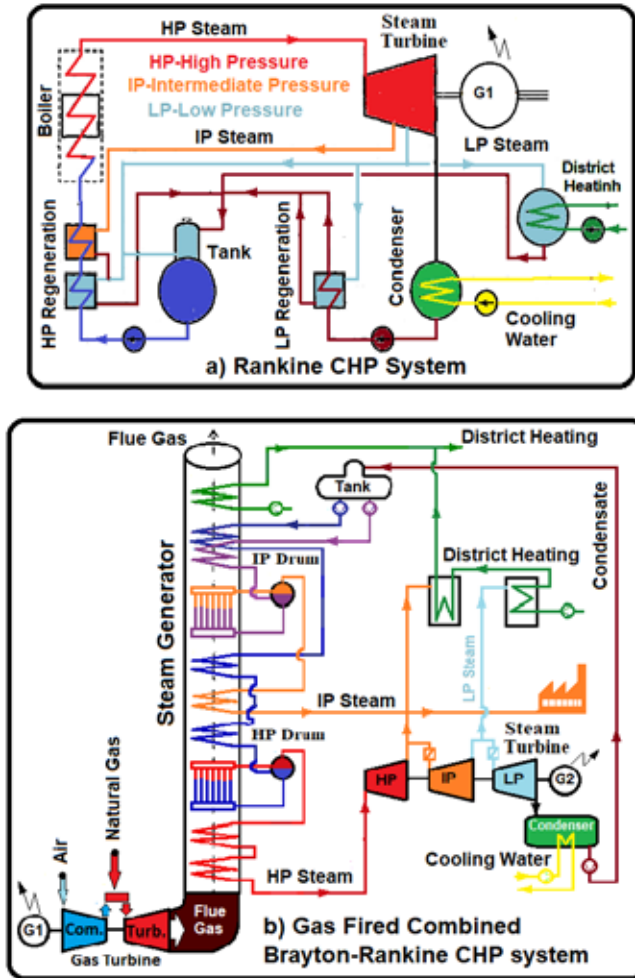


**Figure 5:** a) Rankine CHP system and b) Gas fired combined Brayton-Rankine CHP system

The classic Rankine *CHP* system for increasing the enthalpy of a working medium uses various heat sources, while a boiler is used largely in the combustion of fossil fuels. However, solid fuels and gaseous fuels may burn in a boiler. Gas-fired *CHP* systems, which are intended for achieving high efficiency, are composed of the combined Brayton and Rankine cycle, which is also called the combined gas-steam cycle. The combined gas-steam cycle is composed of a gas turbine, steam generator and turbine condensation system with a thermal station. The combustion of gaseous fuel takes place in a gas turbine. The high temperature of the exhaust gases of a gas turbine, by means of a generator, serves for generating various types of steam and heat for remote heating. The steam is exported from the steam generator to the steam condensing extraction turbine. The extraction steam from the steam turbine is used for industrial purposes, or for remote heating.

The low-carbon property of the gas-steam *CHP* system in comparison to the *CHP* solid fuel system is expressed mainly in the type of fuel, because gaseous fuels contain a lower content of carbon and a higher content of hydrogen. This corresponds to the combustion products of such

fuels, because emissions of  $CO_2$  greenhouse gas are decreased and emissions of water vapour or water are increased. Such gas-steam *CHP* plants can further improve their carbon footprint, because the most recent gas turbine, such as the gas turbine Siemens SGT 800, can, in combination with natural gas, operate with as much as a 75% hydrogen volume fraction [11]. With the further development of steam turbine burners, the hydrogen volume fraction in combination with natural gas will increase further. Likewise, gas turbines can also be powered by biogas.

With the purpose of increasing the ecological focus and promoting the self-supply of the European Union with natural gas, the European Union has established a special Association, the European Clean Hydrogen Alliance [8], which intends, in the first phase, to produce green hydrogen from surplus renewable electricity, and transport it to users with a special methanisation procedure by means of a gas network. Any surplus of green methane will be accumulated in natural gas reservoirs. In the second phase, by the year 2030, the plan is to build gas pipelines which will interconnect hydrogen producers, consumers and reservoirs. Figure 6 shows the development projects of the hydrogen technology and the outline of the hydrogen infrastructure.

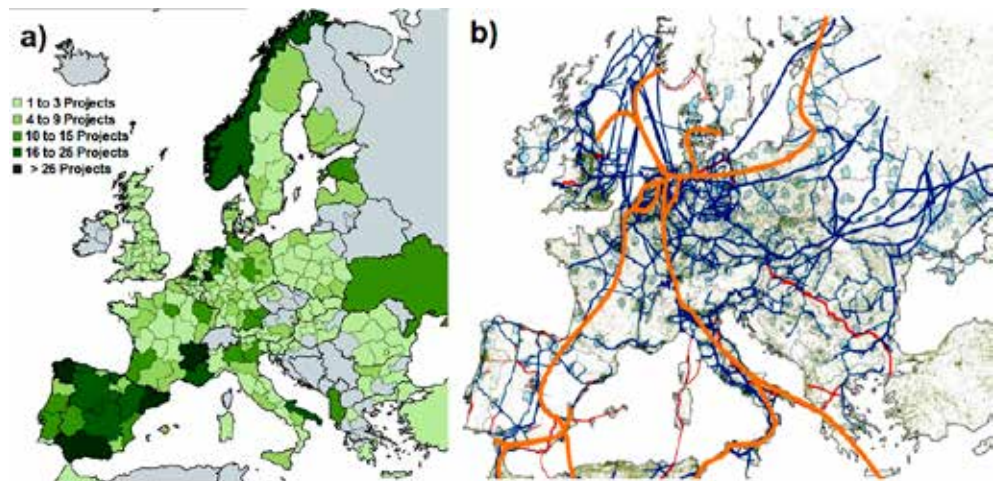


**Figure 6:** a) project pipeline of the European Clean Hydrogen Alliance [12] and b) natural gas infrastructure in Europe (blue and red lines) with the first outline for a hydrogen backbone infrastructure (orange lines) [13]

However, special attention must also be dedicated to the possibility of using the biomass fraction of waste, because the combustion of the fraction increases carbon neutrality. Biomass fraction of waste is formed in waste separation, and is, pursuant to the existing procedures, deposited at landfills or transported to incineration sites, largely abroad. If the biomass fraction of waste is deposited at landfills,  $CO_2$  is produced in the processes of rotting and decay. In case of combustion of the fraction, heat is also generated, which may be used rationally by means of *CHP* systems for the production of electric and thermal energy. For this purpose, the location for the construction of such systems is essential with regard to the utilisation of the already existing infrastructure.

## 4 CONCLUSIONS

Using the model of the *BAT* method of alternative facilities, the article discusses the advantages of energy production by means of *CHP* systems and the low-carbon future of a large *CHP* system. The *BAT* method model is based on the calculation of the saved fuel of a *CHP* system in the event of generation of the same amount of electric and thermal power in alternative facilities. Alternative facilities are facilities where electric and thermal energy are generated separately in separate facilities. The results of the model of the *BAT* method of alternative facilities show that fuel savings of the *CHP* system depend on system load. At a 40% system load, the fuel savings of the *CHP* system equal 27%, and at a 100% system load, the fuel savings of the *CHP* system equal 34%.

The low-carbon transformation of a large *CHP* system is linked intricately to the use of low-carbon or carbon-neutral fuels. Replacement of the fuel type in a *CHP* system is linked intricately to high investment costs. In using gaseous fuel, and in order to reach high efficiency, an appropriate option seems to be gas-steam *CHP* plants. The low-carbon future of the presented plants may be improved further, because the latest gas turbines may, in combination with natural gas, operate with as much as a 75% hydrogen volume fraction, and hydrogen may be obtained from surplus green energy and mixed with natural gas in the methanisation process.

However, special attention must also be paid to the possibility of using the biomass fraction of waste, because the combustion of the fraction increases carbon neutrality. The biomass fraction of waste is currently deposited at landfills or transported to incineration sites, largely abroad. In the case of combustion of the fraction heat is also generated, which may be used rationally by means of *CHP* systems for the production of electric and thermal energy.

## References

- [1] **A. Mambro, F. Congiu, E. Galloni:** *Influence of stage design parameters on ventilation power produced by steam turbine last stage blades during low load operation*, Thermal Science and Engineering Progress, Vol. 28, p. 101054, 2022. Available: <https://doi.org/10.1016/j.tsep.2021.101054>
- [2] **D. Strušnik:** *Integration of machine learning to increase steam turbine condenser vacuum and efficiency through gasket resealing and higher heat extraction into the atmosphere*, International Journal of Energy Research, Vol. 46, Issue 3, 2021. Available: <https://doi.org/10.1002/er.7375>
- [3] **C. Wang, J. Song, W. Zheng, Z. Liu, C. Lin:** *Analysis of economy, energy efficiency, environment: A case study of the CHP system with both civil and industrial heat users*, Case Studies in Thermal Engineering, Vol. 30, p. 101768, 2022. Available: <https://doi.org/10.1016/j.csite.2022.101768>
- [4] **I. Kuštrin, J. Oman, I. Bole:** *Using reference efficiency values of separate heat and power production for allocating fuel cost and carbon dioxide emissions of combined heat and power production*, Konferenca daljinske energetike 2007, Portorož 2007
- [5] **T. Jin:** *The effectiveness of combined heat and power (CHP) plant for carbon mitigation: Evidence from 47 countries using CHP plants*, Sustainable Energy Technologies and Assessments, Vol. 50, p. 101809, 2022

Available: <https://doi.org/10.1016/j.seta.2021.101809>

- [6] **C. Wulf, J. Linßena, P. Zapp:** *Review of Power-to-Gas Projects in Europe*, Energy Procedia, Vol. 155, p.p. 367-378, 2018. Available: <https://doi.org/10.1016/j.egypro.2018.11.041>
- [7] **A. Vargas, A. Sepiúveda-Gálvez, J. D. Barrios-Pérez:** *A fast extremum-seeking approach for the methanisation of organic waste in an anaerobic bioreactor*, IFAC-Papers On Line, Vol. 52, Iss. 1, p.p. 269-274, 2019. Available: <https://doi.org/10.1016/j.ifacol.2019.06.073>
- [8] **European Clean Hydrogen Alliance.** Available: [https://ec.europa.eu/growth/industry/strategy/industrial-alliances/european-clean-hydrogen-alliance\\_sl](https://ec.europa.eu/growth/industry/strategy/industrial-alliances/european-clean-hydrogen-alliance_sl)
- [9] **Directive 2004/8/EC of the European Parliament.** Available: <https://eur-lex.europa.eu/legal-content/EN/TXT/PDF/?uri=CELEX:32004L0008&from=DE>
- [10] **D. Strušnik, M. Golob, J. Avsec:** *Artificial neural networking model for the prediction of high efficiency boiler steam generation and distribution*, Simulation Modelling Practice and Theory, Vol. 57, p.p. 58-70, 2015. Available: <https://doi.org/10.1016/j.simpat.2015.06.003>
- [11] **Siemens Energy.** Available: <https://www.siemens-energy.com/global/en/offerings/power-generation/gas-turbines/sgt-800.html>
- [12] **Project pipeline of the European Clean Hydrogen Alliance.** Available: [https://ec.europa.eu/growth/industry/strategy/industrial-alliances/european-clean-hydrogen-alliance/project-pipeline\\_en](https://ec.europa.eu/growth/industry/strategy/industrial-alliances/european-clean-hydrogen-alliance/project-pipeline_en)
- [13] **Energy post.eu.** Available: <https://energypost.eu/50-hydrogen-for-europe-a-manifesto>

## Abbreviations

<b>BAT</b>	best available technology
<b>CCGT</b>	combined cycle gas turbine
<b>CHP</b>	combined heat and power
<b>CH<sub>4</sub></b>	methane
<b>CO<sub>2</sub></b>	carbon dioxide
<b>HP</b>	high pressure
<b>IP</b>	Intermediate pressure
<b>LP</b>	low pressure

**Parameters**

<b><math>E_{ou\_ALT}</math></b>	total electric power of own use of alternative facilities
<b><math>E_{ou\_CHP}</math></b>	electric power of own use of the <i>CHP</i> system
<b><math>E_{EL}</math></b>	generated electric power
<b><math>LHV</math></b>	lower calorific value of natural gas
<b><math>P_{fuel\_ALT}</math></b>	total fuel power for the production of electric and thermal power of alternative facilities
<b><math>P_{fuel\_CHP}</math></b>	fuel power for electricity and heat production of the <i>CHP</i> system
<b><math>\dot{m}_{fuel}</math></b>	fuel mass flow
<b><math>Q_{DH}</math></b>	generated thermal power of remote heating
<b><math>Q_{IS}</math></b>	generated thermal power of industrial steam
<b><math>S_{fuel}</math></b>	fuel savings
<b><math>P_{fuel_{CHP}}</math></b>	fuel power for electricity and heat production of the <i>CHP</i> system
<b><math>P_{fuel_{DH}}</math></b>	fuel power for the generation of thermal power of remote heating by means of an alternative facility
<b><math>P_{fuel_{IP}}</math></b>	fuel power for the generation of thermal power of industrial steam by means of an alternative facility
<b><math>P_{fuel_E}</math></b>	fuel power for generation of electric power by means of an alternative facility
<b><math>\eta_{DH}</math></b>	efficiency of the alternative facility for the generation of thermal power of remote heating
<b><math>\eta_E</math></b>	efficiency of the alternative facility for generation of electric power
<b><math>\eta_{IS}</math></b>	efficiency of the alternative facility for the generation of thermal power of industrial steam.

# THE IMPACT OF UNBALANCED POWER SUPPLY ON LOAD CURRENTS IN TRANSIENT AND STEADY-STATE OPERATION

## VPLIV NESIMETRIČNIH NAPAVALNIH NAPETOSTI NA TOKE BREMEN MED USTALJENIM OBRATOVANJEM IN MED PREHODNIMI POJAVI

Nina Štumberger<sup>1</sup>, Matej Pintarič<sup>2</sup>, Gorazd Štumberger<sup>2,3\*</sup>

**Keywords:** unbalanced power supply voltages, load currents, steady state, transients, Dommel's method, increase in released heat Abstract

### **Abstract**

The impact of unbalanced power supply voltages on power derating, increases in current values and the heat released from electrical machines and devices is typically analysed in quasi-steady-state operation using sequence components. The ratios between the negative and positive sequence voltage and the homopolar (zero) and positive sequence voltage are used to evaluate the level of voltage unbalance. This paper proposes an extension of this approach that includes subtransient, transient and quasi-steady-state operation of wye (grounded and ungrounded) and delta connected loads, consisting of resistors and magnetically linear and non-linear iron core inductors, which is a novelty. Dommel's method for dynamic simulation of electrical circuits,

---

<sup>3\*</sup> Corresponding author: Professor dr. Gorazd Štumberger, Tel.: +386 (0)2-220-7075, Mailing address: Koroška cesta 46, 2000 Maribor, Slovenia. E-mail address: gorazd.stumberger@um.si, nina.stumberger@rwth-aachen.de

<sup>1</sup> RWTH Aachen University (Rheinisch Westfälische Technische Hochschule), Fakultät für Elektrotechnik und Informationstechnik, Schinkelstr. 2, 52062 Aachen, Germany

<sup>2</sup> University of Maribor, Faculty of Electrical Engineering and Computer Science, Koroška cesta 46, 2000 Maribor, Slovenia

based on the modified nodal potential method, time discretisation and implicit numerical integration, is applied to evaluate the impact of unbalanced power supply voltages on load currents. The magnetically non-linear behaviour of the iron core inductors is accounted for by introducing variable dynamic inductances inside Dommel's method. The integrals of instantaneous values of squared load branch currents values in subtransient, transient and quasi-steady-state operation, determined for different levels of unbalance in supply voltages, are normalised with those calculated for the balanced power supply voltages in quasi-steady-state. The obtained ratios of the integrals are used to implicitly evaluate the impact of unbalance in supply voltages on the increase in released heat due to Joule losses. The proposed approach is generally applicable, while the results are shown for the case study of iron core inductors with magnetically linear and non-linear behaviour.

## **Povzetek**

Vpliv nesimetrije v sinusnih napajalnih napetostih na zmanjšanje moči, povečanje tokov in Joulskih izgub električnih strojev in naprav običajno obravnavamo v kvazi stacionarnih (vnihanih) stanjih, pri tem pa uporabljamo simetrične komponente. Merilo nesimetrije sta najpogosteje razmerji med napetostjo negativnega in pozitivnega ter ničnega in pozitivnega zaporedja simetričnih komponent. To delo predstavlja razširitev opisanega pristopa saj vključuje subtranzientno, tranzientno in kvazi stacionarno območje delovanja v zvezdo in v trikot vezanih bremen, sestavljenih iz zaporedne vezave upora in tuljave z železnim jedrom z magnetno linearnim in magnetno nelinearnim obnašanjem. To je novost, s katero ta prispevek presega obstoječe pristope. Za ovrednotenje vpliva nesimetrije v sinusnih napajalnih napetostih na toke bremen je uporabljena Dommel-ova metoda dinamične simulacije električnih vezij, ki temelji na modificirani metodi vozličnih potencialov, implicitni metodi integracije povezane s časovno diskretizacijo. Magnetno nelinearno obnašanje tuljave z železnim jedrom je upoštevano z uporabo spremenljive dinamične induktivnosti, ki je smiselno integrirana v Dommel-ovo metodo. Integrali kvadratov trenutnih vrednosti tokov bremen, so izračunani za subtranzientno, tranzientno in kvazi stacionarno obratovanje in določeni za različne stopnje nesimetrije v sinusnih napajalnih napetostih. Za potrebe primerjave so podeljeni z vrednostmi integralov kvadratov tokov bremen pri napajanju s simetričnimi sinusnimi napetostmi pri kvazi stacionarnem obratovanju. S tem smo dobili normirano obliko, ki implicitno omogoča ovrednotenje vpliva nesimetrije v sinusnih napajalnih napetostih na toploto sproščeno v obliki Joulskih izgub. Predstavljena metoda je splošno uporabna in jo je mogoče generalizirati, njeno delovanje pa je v tem delu predstavljeno na primeru tuljav z železnim jedrom z magnetno linearnim in z magnetno nelinearnim obnašanjem.

## **1 INTRODUCTION**

With a balanced three-phase power supply, the voltages are sinusoidal, of equal amplitude and phase-shifted to each other by  $120^\circ$ . An uneven distribution of loads over the three phases or errors in the electrical network, such as short circuits, other faults and different unexpected operating conditions, can cause voltage unbalances [1]. The unbalances in voltage supply are usually treated in quasi-steady-state operation of electrical machines and devices using sequence components – the positive (1), the negative (2) and the homopolar (0) component. The level of supply voltage unbalances is evaluated through the ratios of the negative and the homopolar sequence component with respect to the positive one [1], [2].

The supply voltage unbalances can negatively affect the equipment connected to the power supply due to an increase in line currents. This increase causes an increase in Joule losses, which



increases the operating temperature and can cause deterioration of the isolation and negatively affect the lifespan of the equipment [1]. Most of the authors of existing research have focused on the impact of supply voltage unbalances on the quasi-steady-state operation of induction machines. The impact of angle unbalance in supply voltages on operational properties of induction machines is investigated in [3]. The authors in [4, 5] deal with the performance analysis of induction machines supplied with unbalanced sinusoidal voltages in quasi-steady-state operation. The influence of unbalanced sinusoidal and balanced non-sinusoidal supply voltages on the performance of a squirrel-cage induction motor is analysed in [6]. The impact of supply voltage unbalances on the precise derating and energy performance of three-phase induction motors is discussed in [7] and [8] respectively. The modelling effect of supply voltage unbalances in systems with adjustable speed drives is described in [9]. The author in [10] analyses the influence of supply voltage unbalances, combined with over voltages and under voltages, on induction machine winding temperature and loss of insulation life. In [11], the authors deal with thermal effects in the induction machine stator caused by mechanical overloads and supply voltage unbalances. Calorimetric and finite element simulations are applied in [12] to evaluate the impact of supply voltage unbalances on induction motor derating.

Transient operation and magnetically non-linear load behaviour are not considered in any of the aforementioned publications. Although the loads considered in this paper are iron core inductors, the proposed approach is new. It enables the treatment of magnetically linear and non-linear behaviour, including subtransient, transient and quasi-steady-state operation. Using a method similar to the one described in [13], the approach proposed in this paper can be further developed to be suitable for treating iron core inductors and electrical machines.

The aim of this paper is to propose a unified method for evaluating the impact of supply voltage unbalances on the increase in currents and Joule losses of wye and delta connected loads, considering the magnetically linear or non-linear behaviour of the iron core of the load, including subtransient, transient and quasi-steady-state operation.

This paper deals with the impact of supply voltage unbalances on the currents and Joule losses of a three-phase load consisting of iron core inductors connected into the delta, ungrounded and grounded wye. Voltage unbalances of up to 10% are considered. To observe the currents in the transient states as well as in quasi-steady-state operation, the load as well as the supply line are modelled using Dommel's method and simulated in MATLAB. The load model represents iron core inductors with magnetically linear and non-linear behaviour. The iron core saturation is considered by introducing variable dynamic inductance, the value of which decreases when the current reaches a certain threshold. Since the aim of this paper is to explore the effect of supply voltage unbalances on a general load, no specific equipment is considered, although this is an area that could be explored in the future.

The theoretical background for evaluating the supply voltage unbalance and Dommel's method are described in Section 2. Section 3 explains the proposed methodology. The results obtained considering different levels of unbalances in supply voltages in the cases of wye and delta connected iron core inductors with magnetically linear and non-linear behaviour are illustrated in Section 4. In Section 5, the findings are summarised and conclusions are drawn.

## 2 THEORETICAL BACKGROUND

Subsection 2.1 describes the relations among the phasors of phase voltages and sequence component voltages. The latter are used to introduce two factors for evaluating unbalances in sinusoidal supply voltages. Subsection 2.2 provides a comprehensive description of Dommel's method.

### 2.1 Voltage unbalances

Whilst the degree of voltage unbalance can be described in multiple ways, this paper uses the definition of the International Electrotechnical Commission (IEC), which can be found in [2]. It describes how much negative (2) and zero-sequence (0) voltage is superposed on the positive-sequence (1) voltage. The connection between positive-sequence ( $\underline{V}_1$ ), zero-sequence ( $\underline{V}_0$ ), and negative-sequence ( $\underline{V}_2$ ) voltages and the phase voltages ( $\underline{V}_a$ ,  $\underline{V}_b$ ,  $\underline{V}_c$ ) is described by equation (2.1):

$$\begin{bmatrix} \underline{V}_a \\ \underline{V}_b \\ \underline{V}_c \end{bmatrix} = \begin{bmatrix} 1 & 1 & 1 \\ 1 & a^2 & a \\ 1 & a & a^2 \end{bmatrix} \cdot \begin{bmatrix} \underline{V}_0 \\ \underline{V}_1 \\ \underline{V}_2 \end{bmatrix}, \quad (2.1)$$

where  $a = \exp\left(j2\frac{\pi}{3}\right)$  [4].

The voltage unbalance factor (VUF) is defined by the ratio between the negative-sequence and positive sequence voltage, as given by (2.2):

$$\text{VUF} = \frac{V_2}{V_1}. \quad (2.2)$$

Along with the delta and ungrounded wye connection of the load, where zero-sequence voltage unbalance has no effect on the load currents, this paper also deals with the grounded wye connection of the load. Therefore, the zero-sequence voltage unbalance factor (ZSVUF), defined by (2.3):

$$\text{ZSVUF} = \frac{V_0}{V_1} \quad (2.3)$$

is used.

### 2.2 Dommel's method

In order to analyse the transient-state currents, as well as the quasi-steady-state currents, the inductors representing the loads and the connection lines were modelled using Dommel's method, as described in [14]. The basis for this model is the equation for the inductor voltage  $U_L$  given by (2.4):

$$u_L(t) = v_k(t) - v_m(t) = L \frac{d i_{km}}{dt}, \quad (2.4)$$

from which the equation for the inductor current  $i_{km}$ , given in equation (2.5)

$$i_{km}(t) = i_{km}(t-\Delta t) + \frac{1}{L} \int_{t-\Delta t}^t (v_k(\tau) - v_m(\tau)) d\tau \quad (2.5)$$

is derived by integration over a time period  $\Delta t$ .  $t$  is the current point in time,  $\tau$  is an auxiliary variable,  $L$  is the inductance of the inductor while  $v_k(t)$  and  $v_m(t)$  are the potentials on either end of the inductor, as shown in Figure 1.

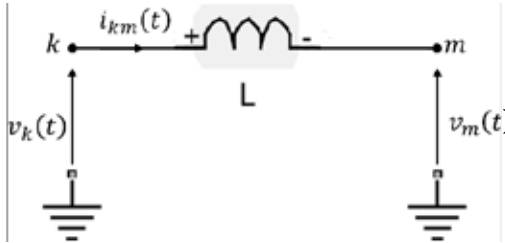


**Figure 1:** Inductor with defined potentials and inductor current

The integral is approximated using the trapezoidal rule, given by (2.6):

$$x(t+\Delta t) = x(t) + \Delta t \frac{1}{2} (f(x(t+\Delta t), t+\Delta t) + f(x(t), t)), \quad (2.6)$$

where  $f$  is the integrated function and  $x$  is the value of the integral.

When the trapezoidal rule (2.6) is applied to (2.5) and the potentials are grouped according to the points in time ( $t$ ,  $t-\Delta t$ ), equation (2.7) is obtained.

$$i_{km}(t) = i_{km}(t-\Delta t) + \frac{\Delta t}{2L} (v_k(t-\Delta t) - v_m(t-\Delta t)) + \frac{\Delta t}{2L} (v_k(t) - v_m(t)) \quad (2.7)$$

It is evident that the inductor current at a given time depends on the inductor current and potential difference over the inductor in the previous time step, and the potential difference over the inductor in the current time step.  $\frac{2L}{\Delta t}$  is a constant and represents the effective resistance of the inductor. The terms describing the conditions in the previous time step can be summarised into the current,  $I_{km}(t-\Delta t)$  which describes the history of the inductor current. Thus, equation (2.7) can be rewritten as equation (2.8)

$$i_{km}(t) = I_{km}(t-\Delta t) + \frac{\Delta t}{2L} (v_k(t) - v_m(t)), \quad (2.8)$$

and the inductor can be modelled as a current source connected in parallel with the effective resistance, as can be seen in the circuit shown in Figure 2.

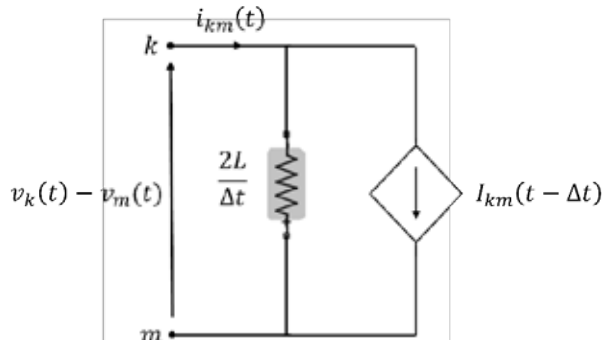


**Figure 2:** Model of an inductor according to Dommel's method

### 3 PROPOSED METHOD

In this section, the circuit models for the different types of load connections are shown. Furthermore, the types and degrees of supply voltage unbalance used in the simulation are described, together with the approach used to consider the magnetically non-linear behaviour of the iron core inductor.

#### 3.1 Circuit models

The circuit model consists of the power supply and connection line, which are the same for all types of load connection, and the load consisting of iron core inductors, which was connected in either delta, ungrounded or grounded wye. The power supply is modelled as a real current source in each of the phases, as can be seen in Figure 3, where the current of a phase  $i_n(t)$  is defined by equation (3.1)

$$i_n(t) = \frac{1}{R} u_n(t), \quad (3.1)$$

where  $R$  is the inner resistance of the current source, which is chosen to be  $10\text{m}\Omega$ .  $u_n(t)$  is the supply voltage of that phase and  $n$  denotes one of the phases, namely 'a', 'b', or 'c',  $n \in \{a,b,c\}$ . The supply voltage is sinusoidal with a frequency of  $50\text{Hz}$  and is defined by (3.2):

$$u_n(t) = \text{Re} \left\{ \sqrt{2} \underline{V}_n \exp(j 2 \pi 50 t) \right\}, \quad (3.2)$$

where  $\underline{V}_n$  denotes the phasor of a phase voltage defined by (2.1). The voltage source is transformed into a current source to enable nodal potential analysis, which is used to calculate the line currents in transient and quasi-steady-state operation.

The connection line supplying the load in each phase is modelled as an inductor, in accordance with Dommel's method, in series with a resistor, as shown in Figure 3. The chosen inductance  $L$  of the connection line is  $0.2\mu\text{H}$ . The resistance of the connection line  $R$  is chosen to equal the internal resistance of the current source, namely  $10\text{m}\Omega$ .

Similarly to the connection line, the load in the form of iron core inductors is also modelled as an RL-combination connected in series for each phase of the load in the case of a wye connection, and each load branch in the case of a delta connection. The iron core inductors are modelled according to Dommel's method as either iron core inductors with magnetically linear behaviour, where the inductance is constant, or iron core inductor with magnetically non-linear behaviour, where iron core saturation is considered by variable dynamic inductance. The discussed circuit models are shown in Figures 3 a) to 3 c). The time  $\Delta t$  interval equals  $1\mu\text{s}$ . The chosen inductances of the iron core inductors  $L_n$ , where  $n$  stands for one of the load phases or branches,  $n \in \{a,b,c\}$ , are  $0.233\text{H}$ . The distinction between the load inductances enables the modelling of the iron core inductors with magnetically non-linear behaviour, which is described in subsection 3.3. The load resistance  $R_l$  is equal in all branches of the load with a value of  $2.08\Omega$ .

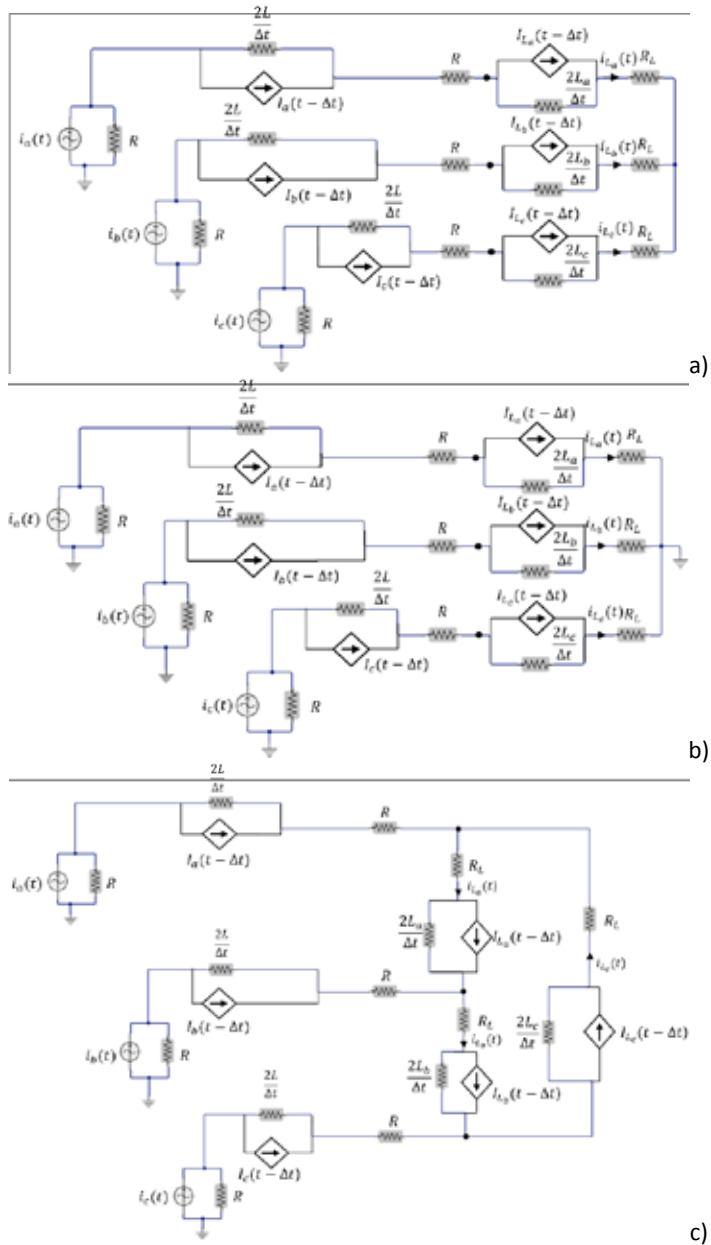


**Figure 3:** Circuits models with the three-phase loads a) ungrounded wye connected, b) grounded wye connected and c) delta connected

To perform the nodal potential analysis, the current vector  $I$  and the admittance matrix  $G$  are determined based on the circuit models. The matrix  $G'$ , which is inverse of  $G$ , is then calculated. Using (3.3)

$$V = G' I, \tag{3.3}$$

the node potential vector  $V$  is determined. Based on this vector, the load currents  $i_{L_n}(t)$  are determined using equation (2.8). To evaluate the Joule losses, the calculated instantaneous current values are recorded for 0.5s in  $1\mu\text{s}$  time intervals  $\Delta t$ . This time interval is divided into three regions: the first is the subtransient region with a duration of 0.1s, the next is the transient region with a duration of 0.3s, and the last is the quasi-steady-state region with a duration of 0.1s. Within each of these regions, the sum of the squared instantaneous values of the load current is calculated using (3.4)

$$i_{n,\text{sum}}^2 = \sum_{k=0}^{\frac{t_{\text{fin}} - t_{\text{exp}}}{\Delta t}} i_{L_n}^2(t_{\text{start}} + k\Delta t). \quad (3.4)$$

To better compare these values in different regions, a sum of squared current values normalised over one period  $i_{n,\text{sum,rel}}^2$  is calculated for all the discussed regions using (3.4) and (3.5):

$$i_{n,\text{sum,rel}}^2 = \frac{i_{n,\text{sum}}^2}{N * i_{n,\text{sum},0}^2}, \quad (3.5)$$

Where  $N$  is the number of periods in the region of observation, while  $i_{n,\text{sum},0}^2$  is the sum of the squared instantaneous current values over one period (20ms) in the quasi-steady-state operation determined for balanced power supply.

Since the Joule losses of the load are proportional to the sum of the squared instantaneous values of the load currents, the normalised sum (3.5) represents the increase of Joule losses over one period compared to those over one period (20ms) in normal quasi-steady-state operation of the load supplied with balanced sinusoidal voltages.

## 3.2 Unbalanced power supply

The negative-sequence and zero-sequence voltage unbalance factors are used to evaluate the level of voltage unbalance. The negative-sequence voltage unbalance factor VUF (2.2) is applied to all three types of load connection, with the VUF ranging from 0 to 10% in 2% intervals. The zero-sequence voltage unbalance factor ZSVUF (2.3) is only applied to the circuit with grounded wye connected load, since it has no effect on the currents of ungrounded wye and delta connected loads. The ZSVUF, defined by (2.3), is increased from 0 to 10% in 2% steps. Additionally, the effect of equal negative-sequence and zero-sequence voltage unbalance simultaneously is investigated for the grounded wye connected load. Figure 4 shows the three-phase supply voltages: the balanced (Figure 4 a)), those with a 10% VUF (Figure 4 b)), those with a 10% ZSVUF (Figure 4 c)), and those with a 10% VUF and a 10% ZSVUF (Figure 4 d)).

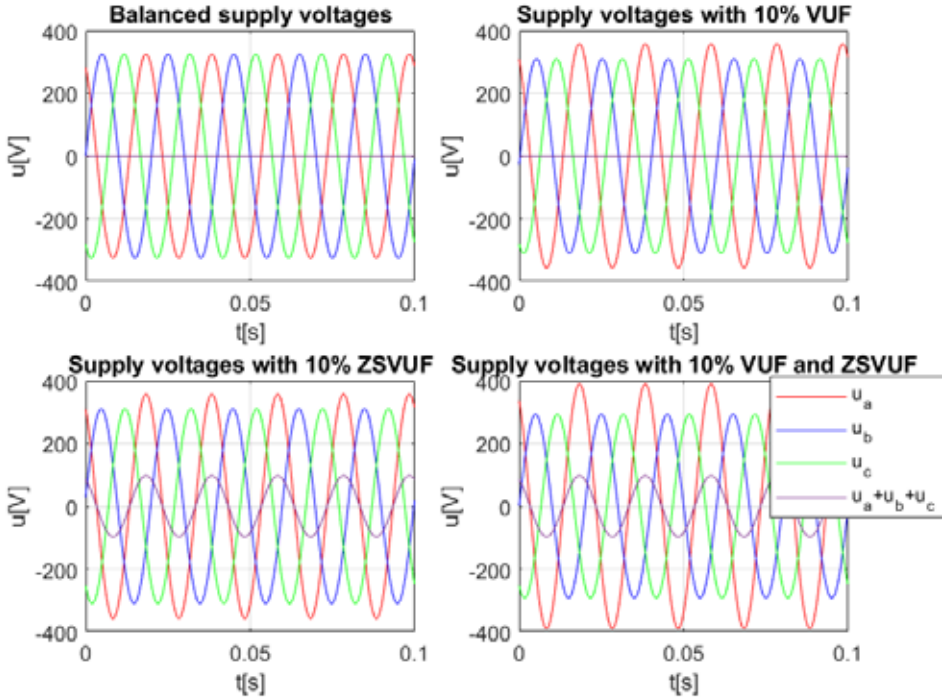


**Figure 4:** Supply voltages  $u_a$ ,  $u_b$ ,  $u_c$  and  $u_a + u_b + u_c$  over time for a) balanced power supply, b) 10% VUF, c) 10% ZSVUF, d) 10% VUF and ZSVUF

### 3.3 Iron core saturation

To model a load consisting of iron core inductors with magnetically non-linear behaviour, the current dependent dynamic inductance  $L_d$  [15] is introduced (3.6):

$$u = \frac{d\Psi(i)}{dt} = \frac{\partial\Psi(i)}{\partial i} \frac{di}{dt} = L_d(i) \frac{di}{dt}, \quad (3.6)$$

where  $\Psi$  is the flux linkage,  $u$  is the voltage over the iron core inductor, and  $i$  the current through the iron core inductor.

In the case of an iron core inductor with magnetically linear behaviour, where iron core saturation does not occur, the load inductance is constant for all currents, with the value  $L_n = 0.233\text{H}$ . In the case of an iron core inductor with magnetically non-linear behaviour, the dynamic inductance decreases when the absolute value of the current through the inductor exceeds the threshold. It is set to 4.5A, which is the amplitude of the load currents in quasi-steady-state operation when supplied with balanced sinusoidal supply voltages. The saturated dynamic inductance is 10 times smaller than the unsaturated one, and has the value  $L_{sn} = 0.0233\text{H}$ . In each step of the simulation, the dynamic inductances of all iron core inductors in the load are adjusted according to the absolute values of the current flowing through them. The inductors used to model the connection lines behave magnetically linearly and have constant values of inductances.

The iron core inductors with magnetically non-linear behaviour, representing the load, are only used for the cases of delta and grounded wye connected loads. In the case of an ungrounded wye connected load, convergency issues might appear, which would require further investigation.

## 4 RESULTS

This section illustrates the results of the simulation. Section 4.1 contains the results for a load containing iron core inductors with magnetically linear behaviour, meaning no saturation effects are considered. Section 4.2 shows the results for a load containing iron core inductors with magnetically non-linear behaviour, meaning saturation effects are considered. All the results are shown in two ways. The first is shown using a graph illustrating the time behaviour of the current in the case of a balanced power supply voltage, and the worst case, meaning the case with the highest voltage unbalance for the discussed case. The second is shown using tables that illustrate the values of the sums of the squared instantaneous current values normalised over one period (3.5) as described in subsection 3.1. They represent an increase in per period Joule losses due to the voltage supply unbalances relative to the per period Joule losses in quasi-steady-state operation in the case of symmetrical supply voltages.

### 4.1 Effects of supply voltage unbalances on iron core inductor loads with magnetically linear behaviour

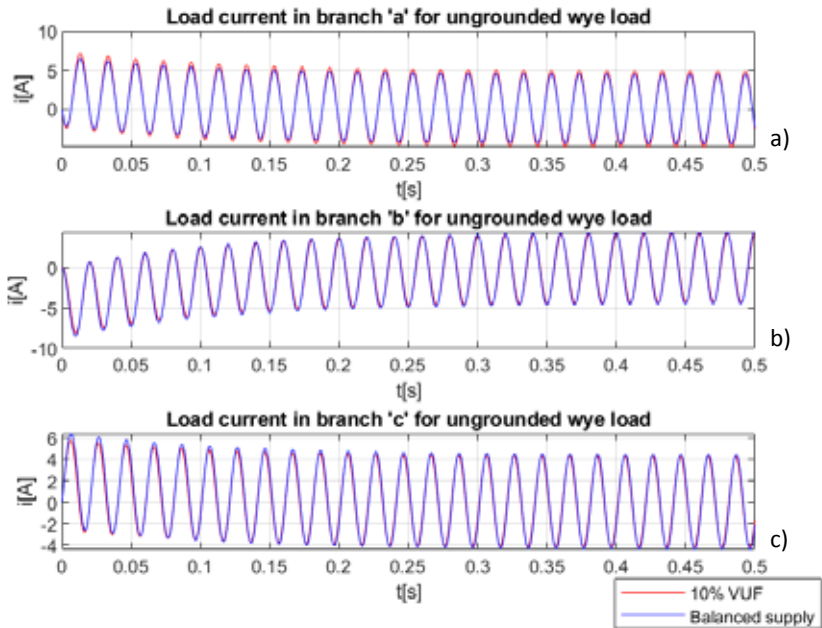
The simulation was initially conducted for the loads consisting of iron core inductors with magnetically linear behaviour, meaning the inductance in each branch of the load was constant.

Figure 5 shows the current over time in each of the load branches for a balanced voltage supply and a supply with a 10% VUF, and the load connected in ungrounded wye. Figures 6 and 7 show the load currents for a grounded wye and delta connected load.

As can be seen in Figures 5 and 6, in the cases of a grounded or ungrounded wye connected load, the negative-sequence voltage unbalance causes an increase in amplitude of the current in phase 'a', compared to operation with a balanced power supply, while the currents in phases 'b' and 'c' decrease. In the cases of a delta connected load, as seen in Figure 7, the amplitude of the current increases in phases 'a' and 'c', and decreases in phase 'b'.

To better illustrate the change in the current time behaviour and its influence on the normalised per period increase in Joule losses, caused by supply voltage unbalances, the level of which is defined by the value of VUF (2.2), the normalised sums of squared instantaneous current values  $i_{n,\text{sum,rel}}^2$  (3.5) are used. The values of  $i_{n,\text{sum,rel}}^2$  in load branches are given in Tables 1 to 3 for all three types of load connection, considering different values of the VUF in the subtransient, transient and quasi-steady-state region of operation. The results shown are completed by the sum of  $i_{n,\text{sum,rel}}^2$  in all three load branches, which represents the total Joule losses in the load.





**Figure 5:** Load currents over time for an ungrounded wye connected load with balanced power supply and a 10% VUF in a) branch 'a', b) branch 'b', and c) branch 'c' of the load

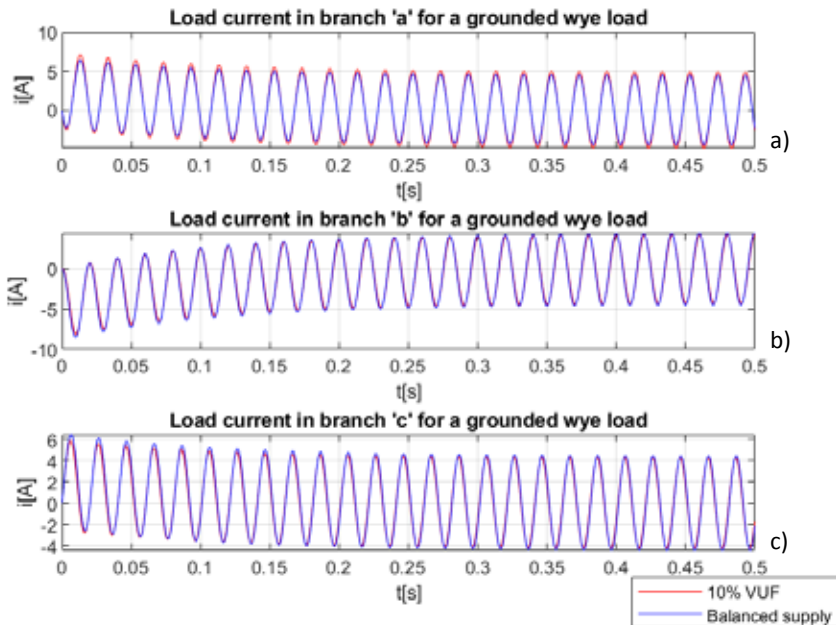


**Figure 6:** Load currents over time for a grounded wye connected load with balanced power supply and a 10% VUF in a) branch 'a', b) branch 'b', and c) branch 'c' of the load

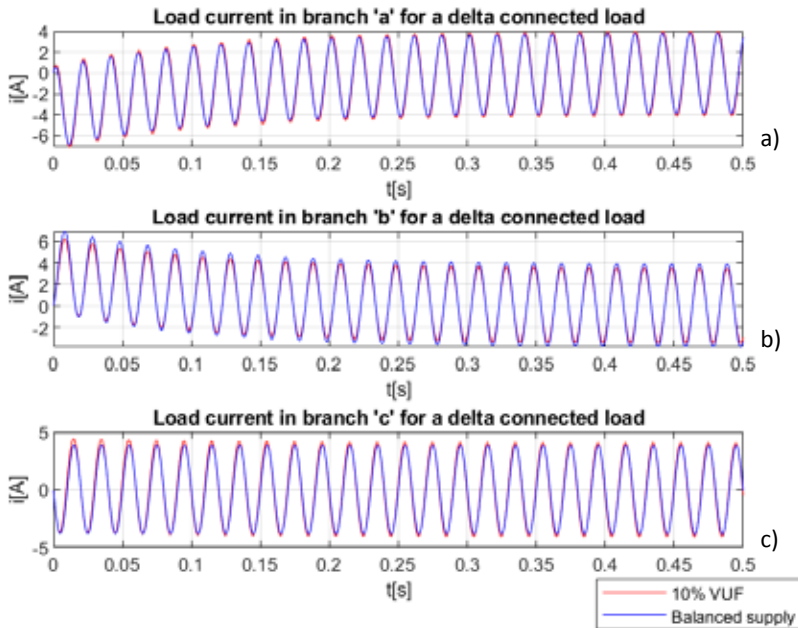


**Figure 7:** Load currents over time for a delta connected load with balanced power supply and a 10% VUF in a) branch ‘a’, b) branch ‘b’, and c) branch ‘c’ of the load

**Table 1:** Relative sum  $i_{n,sum,rel}^2$  for values of VUF between 0 to 10% for an ungrounded wye connected load

VUF [%] $i_{n,sum,rel}^2$	0	2	4	6	8	10
<b>Subtransient</b>						
Branch ‘a’	1.221	1.271	1.321	1.372	1.425	1.478
Branch ‘b’	1.925	1.886	1.849	1.812	1.777	1.742
Branch ‘c’	1.239	1.201	1.164	1.129	1.096	1.064
Total	4.385	4.358	4.334	4.314	4.297	4.284
<b>Transient</b>						
Branch ‘a’	1.010	1.051	1.093	1.135	1.178	1.222
Branch ‘b’	1.060	1.039	1.019	0.999	0.981	0.963
Branch ‘c’	1.019	0.998	0.978	0.959	0.940	0.923
Total	3.089	3.088	3.089	3.093	3.099	3.108
<b>Quasi-steady-state</b>						
Branch ‘a’	1.000	1.040	1.082	1.124	1.166	1.210
Branch ‘b’	1.000	0.980	0.962	0.943	0.926	0.910
Branch ‘c’	1.000	0.980	0.962	0.944	0.926	0.910
Total	3.000	3.001	3.005	3.011	3.019	3.030

**Table 2: Relative sum  $i_{n,sum,rel}^2$  for values of VUF between 0 to 10% for a grounded wye connected load**

VUF [%] $i_{n,sum,rel}^2$	0	2	4	6	8	10
<b>Subtransient</b>						
Branch 'a'	1.209	1.258	1.308	1.359	1.411	1.463
Branch 'b'	1.924	1.885	1.847	1.811	1.775	1.740
Branch 'c'	1.252	1.213	1.176	1.141	1.107	1.074
Total	4.385	4.357	4.332	4.310	4.292	4.277
<b>Transient</b>						
Branch 'a'	1.009	1.050	1.092	1.134	1.177	1.221
Branch 'b'	1.060	1.039	1.019	0.999	0.981	0.963
Branch 'c'	1.020	0.999	0.979	0.960	0.941	0.924
Total	3.089	3.088	3.089	3.093	3.099	3.108
<b>Quasi-steady-state</b>						
Branch 'a'	1.000	1.040	1.082	1.124	1.166	1.210
Branch 'b'	1.000	0.980	0.962	0.943	0.926	0.910
Branch 'c'	1.000	0.980	0.962	0.944	0.926	0.910
Total	3.000	3.001	3.005	3.011	3.019	3.030

**Table 3: Relative sum  $i_{n,sum,rel}^2$  for values of VUF between 0 to 10% for a delta connected load**

VUF [%] $i_{n,sum,rel}^2$	0	2	4	6	8	10
<b>Subtransient</b>						
Branch 'a'	1.667	1.686	1.707	1.728	1.750	1.772
Branch 'b'	1.709	1.641	1.575	1.510	1.446	1.384
Branch 'c'	0.999	1.019	1.040	1.062	1.086	1.111
Total	4.375	4.346	4.321	4.300	4.282	4.268
<b>Transient</b>						
Branch 'a'	1.038	1.058	1.079	1.101	1.123	1.147
Branch 'b'	1.049	1.007	0.966	0.927	0.888	0.849
Branch 'c'	1.000	1.020	1.041	1.063	1.085	1.109
Total	3.087	3.085	3.087	3.090	3.097	3.105
<b>Quasi-steady-state</b>						
Branch 'a'	1.000	1.020	1.042	1.064	1.086	1.110
Branch 'b'	1.000	0.960	0.922	0.884	0.846	0.810
Branch 'c'	1.000	1.020	1.042	1.063	1.086	1.110
Total	3.000	3.001	3.005	3.011	3.019	3.030

As can be seen in Tables 1-3, the relative sum, and with it the Joule losses in the load, increase linearly with the VUF in the quasi-steady-state region of operation. In the cases of a grounded and ungrounded wye connected load, an increase only occurs in branch 'a', with a factor of about 2, meaning a 10% VUF results in a 20% increase in Joule losses in branch 'a'. Whilst the Joule losses in the other two branches decrease, there is still a minor net increase in Joule losses in the load. Similarly, in a delta connected load, the Joule losses increase in branches 'a' and 'c' in accordance with the VUF, meaning a 10% VUF causes a 10% increase in Joule losses in each branch. The Joule losses in branch 'b' decrease, however, there is still a minor net increase in Joule losses, as is the case for the wye connected load.

The results are similar in the transient and subtransient region of operation, namely with the wye connected loads there is an increase in Joule losses in branch 'a' amounting to about twice the VUF, while the losses in the other two phases decrease. Similarly, there is an increase in losses in branches 'a' and 'c' in the delta connected load, and a decrease in branch 'b'. There is minor net increase in Joule losses in all three load connections in the transient region of operation, and a minor decrease in the subtransient region.

These results show that, whilst the total Joule losses in the load increase slightly or even decrease with a higher VUF, the losses in a particular branch increase by a factor of the VUF or twice that, depending on the connection of the load.

The effect of a zero-sequence unbalance on the Joule losses was only observed in the case of a grounded wye connected load. Figure 8 shows the currents in each branch of the load over time for a 10% ZSVUF and balanced power supply. The zero-sequence unbalance in supply voltages does not affect the currents of ungrounded and delta connected loads since there is no path where the zero-sequence current could close.

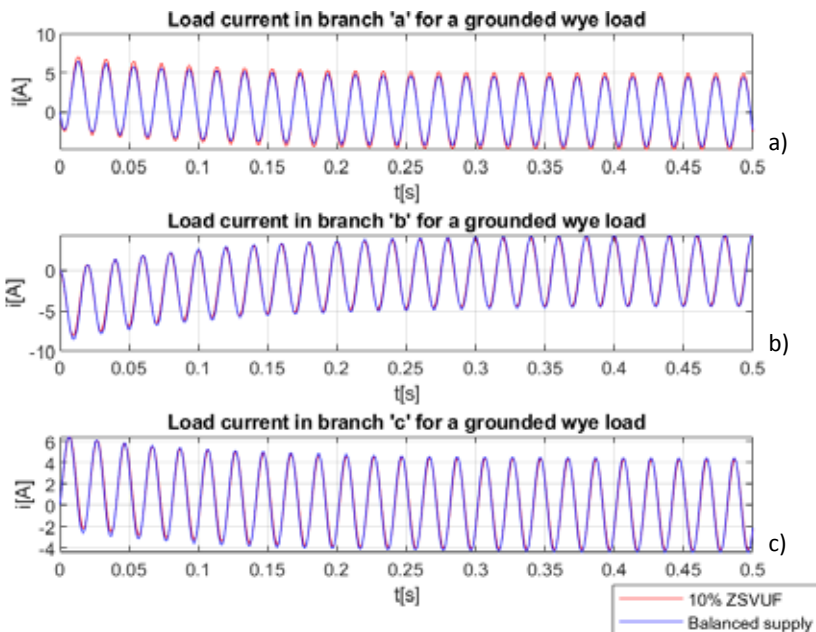


**Figure 8:** Load currents over time for a grounded wye connected load with balanced power supply and a 10% ZSVUF in a) branch 'a', b) branch 'b', and c) branch 'c' of the load

As can be seen in Figure 8, similarly to the negative-sequence voltage unbalance, the zero-sequence voltage unbalance causes an increase in the amplitude of the current in branch 'a', while the amplitude in branches 'b' and 'c' decreases.

The values of  $i_{n,sum,rel}^2$  in the subtransient, transient and quasi-steady-region of operation are shown in Table 4 for different values of the ZSVUF.

**Table 4:** Relative sum  $i_{n,sum,rel}^2$  for values of ZSVUF between 0 to 10% for a grounded wye connected load

ZSVUF [%] $i_{n,sum,rel}^2$	0	2	4	6	8	10
<b>Subtransient</b>						
Branch 'a'	1.209	1.258	1.308	1.359	1.411	1.463
Branch 'b'	1.924	1.887	1.851	1.816	1.782	1.748
Branch 'c'	1.252	1.242	1.232	1.224	1.217	1.210
Total	4.385	4.387	4.391	4.399	4.409	4.422
<b>Transient</b>						
Branch 'a'	1.009	1.050	1.092	1.134	1.177	1.221
Branch 'b'	1.060	1.039	1.019	1.001	0.982	0.965
Branch 'c'	1.020	1.001	0.983	0.966	0.949	0.933
Total	3.089	3.091	3.094	3.100	3.109	3.120
<b>Quasi-steady-state</b>						
Branch 'a'	1.000	1.040	1.082	1.124	1.166	1.210
Branch 'b'	1.000	0.980	0.962	0.944	0.927	0.910
Branch 'c'	1.000	0.980	0.962	0.944	0.926	0.910
Total	3.000	3.001	3.005	3.011	3.019	3.030

As can be seen in Table 4, the ZSVUF has the same effect as the VUF, as shown in Table 2, with an increase in Joule losses of twice the ZSVUF in branch 'a', a decrease in the other two branches and a minor net increase of  $i_{n,sum,rel}^2$  in the transient and quasi-steady-state region of operation. However, there is also a minor net increase in losses in the subtransient region.

Furthermore, the effects of a simultaneous negative-sequence and zero-sequence supply voltage unbalance on the currents of a grounded wye connected load were investigated. Figure 9 shows the currents in each branch for the cases of a 10% VUF and ZSVUF and balanced power supply voltages.

Figure 9 shows an increase in the amplitude of the current in branch 'a' in the case of a voltage unbalance, compared to the case of the balanced voltage supply, and a decrease in the amplitude of the current in the other two branches.

The values of  $i_{n,sum,rel}^2$  for different values of simultaneous VUF and ZSVUF are given in Table 5.

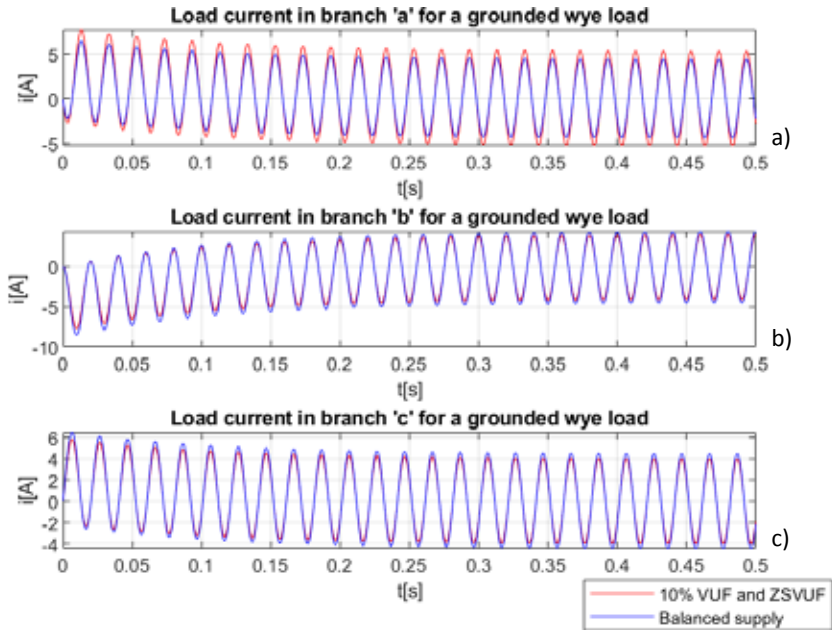


**Figure 9:** Load currents over time for a grounded wye connected load with balanced power supply and a simultaneous 10% ZSVUF and VUF in a) branch 'a', b) branch 'b', and c) branch 'c' of the load

**Table 5:** Relative sum  $i_{n,sum,rel}^2$  for values of simultaneous ZSVUF and VUF between 0 to 10% for a grounded wye connected load

VUF and ZSVUF [%]	0	2	4	6	8	10
$i_{n,sum,rel}^2$						
<b>Subtransient</b>						
Branch 'a'	1.209	1.308	1.411	1.517	1.627	1.741
Branch 'b'	1.924	1.848	1.773	1.700	1.629	1.559
Branch 'c'	1.252	1.202	1.154	1.106	1.060	1.014
Total	4.385	4.358	4.338	4.323	4.315	4.314
<b>Transient</b>						
Branch 'a'	1.009	1.092	1.177	1.266	1.358	1.454
Branch 'b'	1.060	1.018	0.977	0.936	0.897	0.858
Branch 'c'	1.020	0.980	0.940	0.901	0.863	0.826
Total	3.089	3.089	3.094	3.104	3.119	3.138
<b>Quasi-steady-state</b>						
Branch 'a'	1.000	1.082	1.166	1.254	1.346	1.440
Branch 'b'	1.000	0.960	0.922	0.884	0.846	0.810
Branch 'c'	1.000	0.960	0.922	0.884	0.846	0.810
Total	3.000	3.002	3.010	3.022	3.038	3.060

The results shown in Table 5 show that the Joule losses in branch 'a' increase by four times the value of the simultaneous VUF and ZSVUF. As is the case for the VUF and ZSVUF changing separately, there is a decrease in Joule losses in the other two branches of the load, and like the increase in branch 'a', it is about double the decrease in the cases with just a VUF or ZSVUF. The minor net increase of losses in the transient and quasi-steady-state region of operation also doubles, and the minor net decrease in the subtransient region is lower than the case of just a VUF, as shown in Table 2. These results suggest the effects of a negative-sequence and zero-sequence supply voltage unbalance are additive.

The results shown in Tables 1 to 5 represent the relative Joule losses over one period. In order to calculate the total relative losses over the 0.5s period shown in Figures 5 to 9, a sum of the  $i_{n,sum,rel}^2$  values should be formed, with the subtransient value multiplied by 5, the transient  $i_{n,sum,rel}^2$  value multiplied by 15, and the quasi-steady-state  $i_{n,sum,rel}^2$  value multiplied by 5, since that is the number of periods in the three discussed regions.

Due to supply voltage unbalances to an iron core inductor load with linear magnetic behaviour, the Joule losses in one branch can increase by the VUF if the load is connected into delta, twice the VUF if the load is connected into ungrounded wye, and twice the sum of the VUF and ZSVUF when the load is connected into grounded wye.

## 4.2 Effects of supply voltage unbalances on iron core inductor loads with magnetically non-linear behaviour

The simulation was conducted for the loads consisting of iron core inductors with magnetically non-linear behaviour, where variable dynamic inductances were applied to consider the iron core saturation as described in section 3.3. Due to convergence issues, the results for ungrounded wye connected loads are inconclusive and therefore not included in this paper.

Figure 10 shows the load current over time in each branch of the delta connected load for the cases of a balanced power supply, and a 10% VUF, while Figure 11 shows the same results for a grounded wye connected load.

As can be seen in Figures 10 and 11, the currents generally behave similarly to the case with a load with magnetically linear behaviour. Namely, due to the supply voltage unbalance the current amplitude increases in branch 'a' and decreases in the other two branches for the grounded wye connected load, whilst it increases in branches 'a' and 'c', and decreases in branch 'b' for the delta connected load. However, the decrease in the dynamic inductance due to the saturation, after reaching the saturation value of the current, causes a rapid increase in the current amplitude. This can be observed in the subtransient and partially the transient region of operation for both load connections. Additionally, in the case of the grounded wye connected load, the effects of saturation are also visible in the quasi-steady-state region of operation in branch 'a', when the VUF is 10%, since the current increase due to the supply voltage unbalance causes the current to reach values above the saturation threshold. This is not the case for the delta connected load, due to the current increase being in both branches 'a' and 'c' with a lower value.

To better present the impact of these effects on current responses and thus Joule losses, the relative sums  $i_{n,sum,rel}^2$  are given in Table 6 for the delta connected load and in Table 7 for the grounded wye connected load.

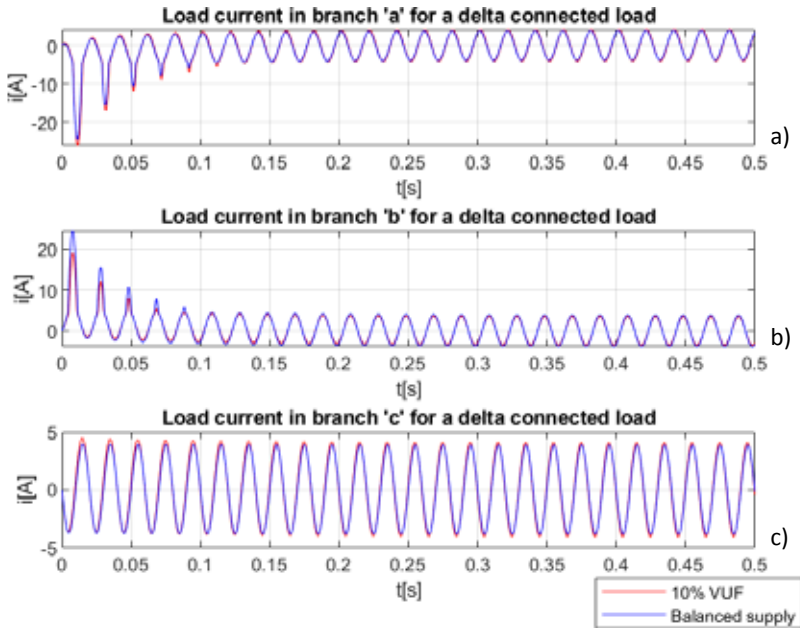


**Figure 10:** Load currents over time for a delta connected iron core inductor with magnetically non-linear behaviour with a balanced voltage supply and a 10% VUF in a) branch ‘a’, b) branch ‘b’, and c) branch ‘c’ of the load

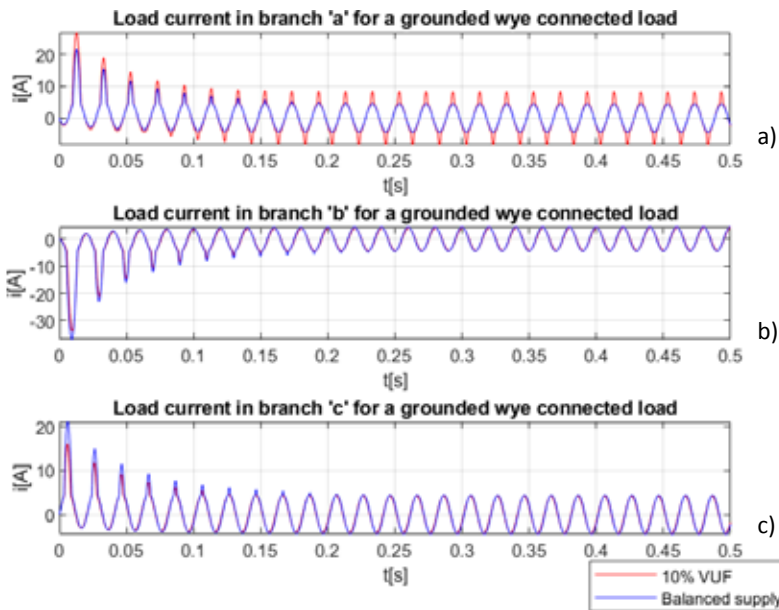


**Figure 11:** Load currents over time for a grounded wye connected iron core inductor with magnetically non-linear behaviour with a balanced voltage supply and a 10% VUF in a) branch ‘a’, b) branch ‘b’, and c) branch ‘c’ of the load



**Table 6:** Relative sum  $i_{n,sum,rel}^2$  for values of VUF between 0 to 10% for a delta connected iron core inductor load

VUF [%] $i_{n,sum,rel}^2$	0	2	4	6	8	10
<b>Subtransient</b>						
Branch 'a'	5.446	5.611	5.777	5.968	6.143	6.344
Branch 'b'	5.468	4.957	4.481	4.026	3.613	3.222
Branch 'c'	0.999	1.019	1.040	1.063	1.087	1.113
Total	11.913	11.587	11.298	11.057	10.843	10.679
<b>Transient</b>						
Branch 'a'	1.010	1.030	1.051	1.073	1.096	1.120
Branch 'b'	1.015	0.977	0.939	0.903	0.866	0.831
Branch 'c'	1.000	1.020	1.041	1.063	1.085	1.109
Total	3.025	3.027	3.031	3.038	3.048	3.060
<b>Quasi-steady-state</b>						
Branch 'a'	1.000	1.020	1.042	1.064	1.086	1.110
Branch 'b'	1.000	0.960	0.922	0.884	0.847	0.810
Branch 'c'	1.000	1.020	1.042	1.063	1.086	1.110
Total	3.000	3.001	3.005	3.011	3.019	3.030

**Table 7:** Relative sum  $i_{n,sum,rel}^2$  for values of VUF between 0 to 10% for a grounded wye connected iron core inductor load

VUF [%] $i_{n,sum,rel}^2$	0	2	4	6	8	10
<b>Subtransient</b>						
Branch 'a'	3.504	3.860	4.249	4.667	5.068	5.535
Branch 'b'	9.951	9.579	9.199	8.855	8.507	8.182
Branch 'c'	3.387	3.095	2.813	2.553	2.311	2.087
Total	16.843	16.534	16.261	16.075	15.885	15.804
<b>Transient</b>						
Branch 'a'	1.023	1.087	1.206	1.391	1.636	1.942
Branch 'b'	1.052	1.024	0.998	0.975	0.954	0.934
Branch 'c'	1.027	1.001	0.978	0.956	0.936	0.918
Total	3.102	3.112	3.182	3.322	3.526	3.794

VUF [%] $i_{n,sum,rel}^2$	0	2	4	6	8	10
<b>Quasi-steady-state</b>						
Branch 'a'	1.000	1.054	1.188	1.385	1.637	1.943
Branch 'b'	1.000	0.980	0.962	0.944	0.926	0.910
Branch 'c'	1.000	0.980	0.962	0.944	0.927	0.910
Total	3.000	3.014	3.112	3.273	3.490	3.763

The comparison of the results shown in Tables 3 and 6 shows that in the quasi-steady-state region of operation there is no difference between the relative sum  $i_{n,sum,rel}^2$  of the delta connected iron core inductors with magnetically linear and non-linear behaviour, due to the currents remaining below the saturation threshold even in the case of unbalanced supply voltages. This is not the case with the grounded wye connected load, as can be seen from Tables 2 and 7. Whilst the decrease in Joule losses ( $i_{n,sum,rel}^2$ ) in branches 'b' and 'c' remains equal for the iron core inductors with magnetically linear and non-linear behaviour, the increase in Joule losses in branch 'a' is not linear but instead approximately proportional to the square of the VUF. This causes the Joule losses to nearly double in the case of a 10% VUF compared to the case of a balanced power supply. This subsequently leads to larger increase in net Joule losses in the load.

The results are similar in the transient region of operation, with the losses in the case of the delta connected load (Table 6) remaining approximately equal to those in Table 3. In the case of a wye connected load, the Joule losses increase proportional to the square of the VUF (Table 7). In the

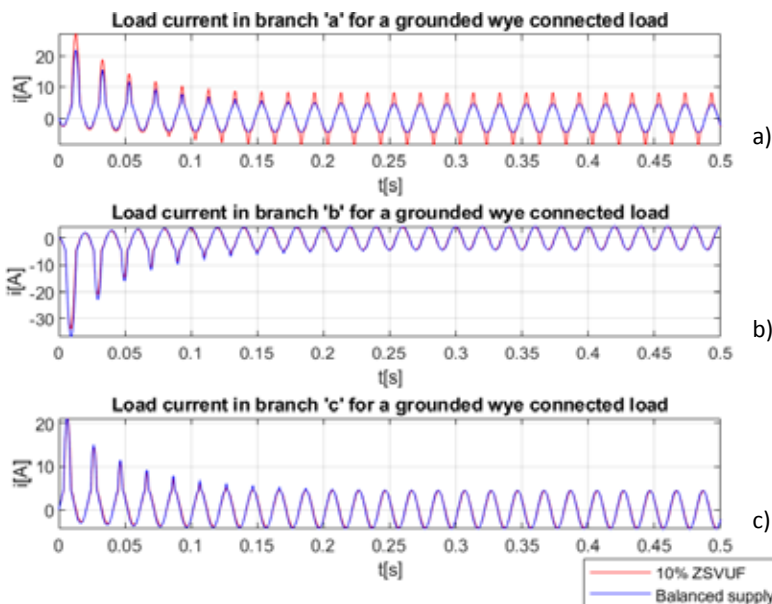


**Figure 12:** Load currents over time for a grounded wye connected iron core inductor with magnetically non-linear behaviour with a balanced voltage supply and a 10% ZSVUF in a) branch 'a', b) branch 'b', and c) branch 'c' of the load

subtransient region, the saturation effects are visible in both loads – the grounded wye and delta connected iron core inductors with magnetically non-linear behaviour (Tables 6 and 7) – due to the currents surpassing the saturation threshold. This causes a larger increase in the Joule losses in branches ‘a’ and ‘c’ of the delta connected load and in branch ‘a’ of the wye connected load. However, these increases are not proportional to the square of the VUF as in the case of the transient or quasi-steady-state region with the wye connected load. Additionally, the relative Joule losses are generally much higher compared to the load with magnetically linear behaviour, even in the balanced case. Even though the total losses increase in general, they decrease with the VUF in a similar way as in the case with a load with magnetically linear behaviour (Tables 2 and 3).

The effects of zero-sequence voltage unbalance can be seen in Figure 12, which shows the load currents over time in a grounded wye connected iron core inductor load with magnetically non-linear behaviour for a 10% ZSVUF and balanced supply voltages.

It is evident from Figure 12 that a zero-sequence voltage unbalance has a similar effect on the current responses as the negative-sequence voltage unbalance seen in Figure 11. The effects of the magnetically non-linear behaviour of the iron core inductor on the relative sum  $i_{n,sum,rel}^2$  can be seen in the subtransient and partially transient region of operation in all three branches in the case of the unbalanced and balanced power supply, whilst in quasi-steady-state region it is only present in branch ‘a’ in the case of a supply voltage unbalance.

The relative sum  $i_{n,sum,rel}^2$  for values of the ZSVUF between 0 and 10% are shown in Table 8.

**Table 8:** Relative sum  $i_{n,sum,rel}^2$  for values of ZSVUF between 0 to 10% for a grounded wye connected iron core inductor load

ZSVUF [%] $i_{n,sum,rel}^2$	0	2	4	6	8	10
<b>Subtransient</b>						
Branch ‘a’	3.504	3.860	4.249	4.667	5.068	5.535
Branch ‘b’	9.940	9.572	9.207	8.850	8.527	8.192
Branch ‘c’	3.387	3.357	3.328	3.299	3.281	3.272
Total	16.832	16.789	16.784	16.816	16.875	16.998
<b>Transient</b>						
Branch ‘a’	1.023	1.087	1.206	1.391	1.636	1.942
Branch ‘b’	1.052	1.024	0.999	0.976	0.955	0.935
Branch ‘c’	1.027	1.002	0.980	0.960	0.941	0.923
Total	3.102	3.113	3.185	3.326	3.532	3.800
<b>Quasi-steady-state</b>						
Branch ‘a’	1.000	1.054	1.188	1.385	1.637	1.943
Branch ‘b’	1.000	0.980	0.962	0.944	0.926	0.910
Branch ‘c’	1.000	0.980	0.962	0.944	0.927	0.910
Total	3.000	3.014	3.112	3.273	3.491	3.764

Similarly to the effects of the VUF, the ZSVUF causes an increase of  $i_{n,\text{sum,rel}}^2$  and thus the Joule losses in branch 'a', which is proportional to the square of the ZSVUF in the transient and quasi-steady-state region of operation. However, the decrease in Joule losses in branches 'b' and 'c' in Table 8 remains the same as in the case with the load with magnetically linear behaviour, causing a higher increase in the total Joule losses in these regions than in Table 4. In the subtransient region, a larger increase in total Joule losses is also noticeable, compared to Table 4, however, unlike the values in Table 7, the total losses increase with the ZSVUF, as was in the case with a grounded wye connected load with magnetically linear behaviour (Table 4).

The effects of a simultaneous negative-sequence and positive sequence voltage unbalance are shown in Figure 13, which shows the load currents over time in a grounded wye connected iron core inductor load with magnetically non-linear properties for a simultaneous 10% ZSVUF and VUF and balanced power supply.

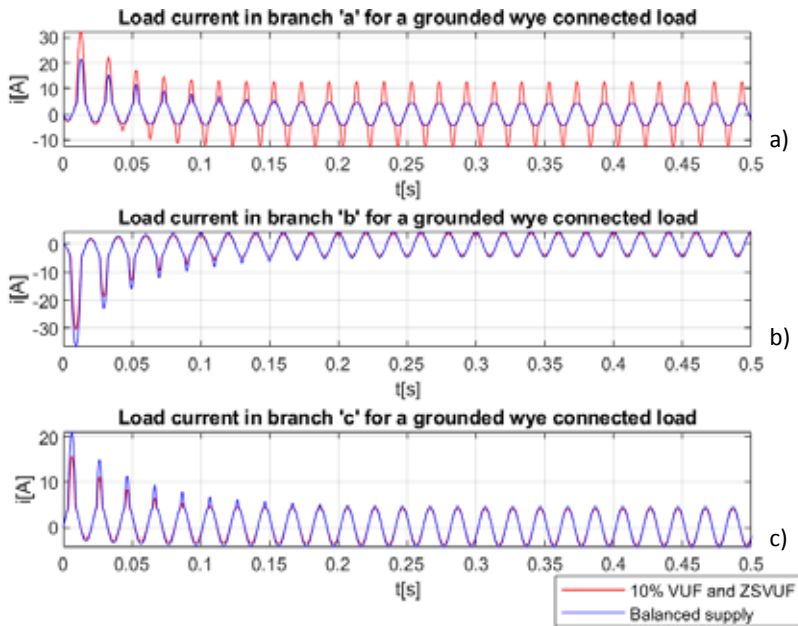


**Figure 13:** Load currents over time for a grounded wye connected iron core inductor with magnetically non-linear behaviour with balanced power supply and a simultaneous 10% ZSVUF and VUF in a) branch 'a', b) branch 'b', and c) branch 'c' of the load

As seen in Figure 13, the amplitude of the current in branch 'a' increased compared to the cases seen in Figures 11 and 12, however, the overall behaviour remains the same.

Table 9 shows the relative sums  $i_{n,\text{sum,rel}}^2$  representing the Joule losses.

**Table 9:** Relative sum  $i_{n,sum,rel}^2$  for values of simultaneous ZSVUF and VUF between 0 to 10% for a grounded wye connected iron core inductor load

VUF and ZSVUF [%] $i_{n,sum,rel}^2$	0	2	4	6	8	10
<b>Subtransient</b>						
Branch 'a'	3.504	4.249	5.068	6.032	7.191	8.533
Branch 'b'	9.951	9.186	8.462	7.770	7.102	6.483
Branch 'c'	3.387	3.051	2.736	2.444	2.176	1.920
Total	16.843	16.486	16.265	16.246	16.469	16.936
<b>Transient</b>						
Branch 'a'	1.023	1.206	1.636	2.306	3.215	4.353
Branch 'b'	1.052	0.996	0.949	0.904	0.862	0.823
Branch 'c'	1.027	0.978	0.933	0.892	0.854	0.818
Total	3.102	3.180	3.518	4.102	4.932	5.994
<b>Quasi-steady-state</b>						
Branch 'a'	1.000	1.188	1.637	2.311	3.226	4.361
Branch 'b'	1.000	0.960	0.922	0.884	0.846	0.810
Branch 'c'	1.000	0.961	0.922	0.884	0.847	0.810
Total	3.000	3.109	3.481	4.078	4.919	5.982

The results shown in Table 9 indicate that the simultaneous negative-sequence and zero-sequence voltage unbalances result in an increase in Joule losses in branch 'a' of the load, which is proportional to approximately double the square value of the VUF and ZSVUF in the transient and quasi-steady-state region. In the case of a 10% simultaneous VUF and ZSVUF this means more than four times the Joule losses in that branch than in the case of a balanced power supply. Furthermore, due to the losses not increasing in other branches compared to the case with a load with magnetically linear behaviour (Table 5), compared to the case with a balanced power supply, the total losses almost doubled as well. In the subtransient region, the Joule losses in branch 'a' also increased compared to Table 5, although not proportional to the square value of the VUF and ZSVUF. At a 10% zero-sequence and negative-sequence voltage unbalance, the losses in branch 'a' are more than double those in the case of a balanced power supply. Additionally, due to the larger increase in losses caused by the zero-sequence voltage unbalance, the total Joule losses slightly increased with the VUF and ZSVUF. These results suggest that the effects of the VUF and ZSVUF are additive in the case of an iron core inductor load with magnetically non-linear behaviour.

The results show that due to supply voltage unbalances of an iron core inductor load with magnetically linear behaviour, the Joule losses in one branch, compared to the case of a balanced power supply, can increase by the VUF if the load is connected into delta, and twice the sum of the square values of the VUF and ZSVUF when the load is connected into grounded wye. This

means that in a grounded wye connected load with magnetically non-linear behaviour, even small supply voltage unbalances can lead to a larger loss of efficiency and overheating.

## 5 CONCLUSION

This work proposes a unified method for evaluating the impact of supply voltage unbalances on the increase in currents and Joule losses of wye and delta connected loads. It considers the magnetically linear or non-linear behaviour of iron core conductors in subtransient, transient and quasi-steady-state operation. The supply voltage unbalances are characterised by the VUF and ZSVUF. The proposed method is based on Dommel's method, which utilises a modified nodal potential method, implicit numerical integration and time discretisation for dynamic and quasi-steady-state simulations of electric circuits. The magnetically non-linear behaviour of iron core inductors is considered in the form of variable current dependent dynamic inductances.

Although the proposed method is demonstrated in the case studies of wye and delta connected loads consisting of iron core inductors with magnetically linear and non-linear behaviour, it can be extended towards applicability to electrical machines. The results presented in the paper clearly show to what extent the supply voltage unbalances influence the currents in the branches and corresponding Joule losses of the discussed loads in subtransient, transient and quasi-steady-state operation.

## References

- [1] **A. von Jouanne, B. Banerjee:** *Assessment of voltage unbalance*, IEEE Transactions on Power Delivery, vol.16, no. 4 pp.782-790, 2001
- [2] **IEEE STANDARDS ASSOCIATION:** *IEEE Recommended Practice for Monitoring Electric Power Quality*, IEEE, p.p.25-28, 2019, DOI: 10.1109/IEEESTD.2019.8796486
- [3] **Y. Wang:** *Analysis of effects of three-phase voltage unbalance on induction motors with emphasis on the angle of the complex voltage unbalance factor*, IEEE Transactions on Energy Conversion, vol.16, no.3, p.p.270-275, 2001
- [4] **Y. Wang:** *An analytical study on steady-state performance of an induction motor connected to unbalanced three-phase voltage*, 2000 IEEE Power Engineering Society Winter Meeting. Conference Proceedings, p.p.159 – 164, 2000
- [5] **J. Faiz, H. Ebrahimpour, P. Pillay:** *Influence of unbalanced voltage on the steady-state performance of a three-phase squirrel-cage induction motor*, IEEE Transactions on Energy Conversion, vol.19, no.4, pp.657-662, 2004
- [6] **C. T. Raj, P. Agarwal, S. P. Srivastava:** *Performance Analysis of a Three-Phase Squirrel-Cage Induction Motor under Unbalanced Sinusoidal and Balanced Non-Sinusoidal Supply Voltages*, 2006 International Conference on Power Electronic, Drives and Energy Systems, p.p.1-4, 2006
- [7] **J. Faiz, H. Ebrahimpour:** *Precise derating of three-phase induction motors with unbalanced voltages*, Fourtieth IAS Annual Meeting. Conference Record of the 2005 Industry Applications Conference, p.p.485-491, 2005

- [8] **E. C. Quispe, I. D. Lopez:** *Effects of unbalanced voltages on the energy performance of three-phase induction motors*, 2015 IEEE Workshop on Power Electronics and Power Quality Applications (PEPQA), p.p.1-6, 2015
- [9] **K. Lee, G. Venkataramanan, T. M. Jahns:** *Modeling Effects of Voltage Unbalances in Industrial Distribution Systems With Adjustable-Speed Drives*, IEEE Transactions on Industry Applications, vol.44, no.5, p.p.1,322-1,332, 2008
- [10] **P. Gnacinski:** *Windings Temperature and Loss of Life of an Induction Machine Under Voltage Unbalance Combined With Over- or Undervoltages*, IEEE Transactions on Energy Conversion, vol.23, no.2, p.p.363-371, 2008
- [11] **J. L. Gonzalez-Cordoba, R. A. Osornio-Rios, D. Granados-Lieberman, R. D. J. Romero-Troncoso, M. Valtierra-Rodriguez:** *Correlation Model Between Voltage Unbalance and Mechanical Overload Based on Thermal Effect at the Induction Motor Stator*, IEEE Transactions on Energy Conversion, vol.32, no.4, pp.1,602-1,610, 2017
- [12] **P. Sudasinghe, U. Jayatunga, P. Commins, J. Moscrop, S. Perera:** *Dependancy of Three Phase Induction Motor Derating Aspects on Complex Voltage Unbalance Factor: A Calorimetric and Finite Element Simulation Study*, IEEE Access, vol.9, p.p.147,063-147,071, 2021
- [13] **G. Štumberger, B. Štumberger, T. Maričič:** *Magnetically nonlinear dynamic models of synchronous machines and experimental methods for determining their parameters*, Energies, vol.12, no.18, p.p.1-22, 2019
- [14] **J. Arrillaga,** *Computer modelling of electrical power systems*, Wiley, 2001
- [15] **G. Štumberger, Ž. Plantić, B. Štumberger, T. Maričič:** *Impact of static and dynamic inductance on calculated time response*, Przegląd Elektrotechniczny, vol.87, iss. 3, p.p.190-193, 2011

## Nomenclature

(Symbols)	(Symbol meaning)
$\underline{V}_0$	Phasor of the zero-sequence voltage
$\underline{V}_1$	Phasor of the positive-sequence voltage
$\underline{V}_2$	Phasor of the negative-sequence voltage
$\underline{V}_a$	Phasor of the voltage phase voltage in phase 'a'
$\underline{V}_b$	Phasor of the voltage phase voltage in phase 'b'
$\underline{V}_c$	Phasor of the voltage phase voltage in phase 'c'
$exp$	Exponential function
$a$	$exp\left(j2\frac{\pi}{3}\right)$

## Nomenclature

(Symbols)	(Symbol meaning)
$j$	Imaginary unit
$VUF$	Voltage unbalance factor
$ZSVUF$	Zero sequence voltage unbalance factor
$u_L(t)$	Inductor voltage
$v_k(t)$	Potential in point $k$
$v_m(t)$	Potential in point $m$
$i_{km}(t)$	Inductor current at time $t$
$L$	Inductance
$t$	Time
$\Delta t$	Time period
	Auxiliary variable
$f(x(t), t)$	Integrated function
$x(t)$	Value of the integral of function $f$
$I_{km}(t-\Delta t)$	Current describing the history of the inductor current
$i_n(t)$	Current of a phase
$u_n(t)$	Supply voltage of a phase
$n$	Index denoting one of the phases, $n \in \{a, b, c\}$
$R$	Resistance of the current source and cable
$\underline{V}_n$	Phasor of the supply voltage of phase $n$
$L_n$	Inductance of the iron core inductor in branch $n$
$R_L$	Load resistance
$I$	Current vector
$G$	Impedance matrix
$G'$	The inverse of the impedance matrix
$V$	Node potential vector
$i_{L_n}(t)$	Load current in branch $n$
$i_{n, \text{sum}}^2$	The sum of the squared instantaneous value of the load current in branch $n$



## Nomenclature

(Symbols)	(Symbol meaning)
$t_{\text{start}}$	Start time of a region of operation
$t_{\text{stop}}$	Stop time of a region of operation
$i_{n,\text{sum,rel}}^2$	Sum of the squared instantaneous values of the load current in branch $n$ normalised over one period
$N$	Number of periods
$i_{n,\text{sum},0}^2$	The sum of the squared instantaneous value of the load current in branch $n$ during a balanced power supply and quasi-steady-state region of operation
$\Psi$	Flux linkage
$L_{\text{dn}}$	Dynamic inductance of the load in branch $n$



# REDUCING CARBON FOOTPRINT IN AN OEM SUPPLY CHAIN CAUSED BY INADEQUATE INTERPRETATION OF X-RAY RESULTS OF HIDDEN DEFECTS IN DUCTILE IRON CASTINGS

## ZMANJŠANJE OGLJIČNEGA ODTISA V DOBAVNI VERIGI OEM-OV ZARADI NEUSTREZNE INTERPRETACIJE REZULTATOV RTG SKRITIH NAPAK V NODULARNI LITINI

Tadej Pavlin<sup>1</sup><sup>✉</sup>, Iztok Brinovar<sup>1</sup>, Bojan Stergar<sup>1</sup>, Zdravko Praunseis<sup>1</sup>

**Keywords:** carbon footprint, ductile iron, X-ray inspection, cutting inspection, hidden mistakes, defects, porosity, inclusion, green energy, reduction in energy production

### **Abstract**

In the global market, the casting industry recorded a growth trend for ductile iron last year. Ductile iron is used due to its excellent mechanical properties, machinability and castability. The microstructure of nodular cast iron consists of a metal matrix and graphite extruded in the form of beads and nodules. In recent years, the production of ductile iron castings has increased significantly for parts for heavy transport vehicles and containers for permanent disposal of nuclear

<sup>✉</sup> Corresponding author: PhD student, Tadej Pavlin, Faculty of Energy Technology, University of Maribor, Tel: +386 (0)37 770 400, Mailing address: Koroška cesta 62a, Velenje, Slovenia, E-mail address: tadej.pavlin@livar.si

<sup>1</sup> University of Maribor, Faculty of Energy technology, Koroška cesta 62a, Velenje, Slovenia

waste, and it is expected that this trend of expansion will continue for at least the next twenty years. When poured in sand moulds, the quality of products can not be reached. There can be defects on the raw surface and/or on the machining surface, as well as hidden defects inside the material. For casting products, defects can be detected on raw and machining surfaces and inside material defects by carrying out a visual inspection. The results of the inspection depend on the inspection method used. In general, basic methods of cutting or milling inspection are used in the casting industry, which means that products are classified in terms of whether or not they meet the drawing specification(s). The authors of this paper focused on the hidden defects inside ductile iron material, which can be detected by carrying out a cutting or milling inspection or through an X-ray inspection. Huge amounts of energy and energy sources are used in the production of nodular cast iron, which creates a negative environmental footprint. Therefore, by being preventively rational and through appropriate control procedures it is possible to significantly reduce the carbon footprint.

## **Povzetek**

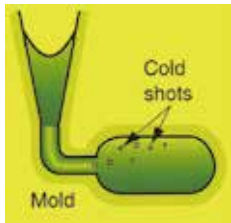
V livarski industriji se v zadnjih letih na svetovnem trgu soočajo s trendom rasti uporabe nodularne litine. Nodularna litina se uporablja zaradi zelo dobrih mehanskih lastnosti, dobre obdelovalnosti in dobre ulivne sposobnosti. Mikrostruktura nodularnega litine je sestavljena iz kovinske matrice in grafita, ekstrudiranega v obliki kroglic, nodul. V zadnjih letih se je močno povečala proizvodnja nodularnih litin za dele, kot so težka transportna vozila, zabojnike za trajno odlaganje jedrskih odpadkov in pričakujemo, da se bo ta trend širitve nadaljeval vsaj naslednjih dvajset let, ker gre za naj boljši približek jeklu. V litrski industriji je bilo splošno znano, da pri vlivanju v pesek nikoli ne dosežemo 100% kakovosti izdelkov, lahko so prisotne napake na surovi površini, na obdelovalni površini ali minimalno vedno lahko prisotne skrite napake znotraj materiala. Pri izdelku za ulivanje lahko z vizualnim pregledom zaznamo napake na surovi in obdelovalni površini ter notranjo napako v materialu, odvisno je le, na kateri način pregleda dobimo rezultat pregleda. V splošnih primerih industrije litja lahko uporabimo osnovne metode pregleda rezanja ali struženja. To pomeni, da so izdelki v skladu s specifikacijo risbe ali ne. V članku je raziskava osredotočena na skrite napake v notranjosti nodularne litine, ki jih je mogoče odkriti z rezalnim ali rezkalnim pregledom ali z rentgenskim pregledom. Pri izdelavi nodularne litine se uporabi izredno veliko energije in energentov zato imamo prisoten tudi velik pečat odličnega odtisa na okolje v negativnem smislu. Zato smo lahko preventivno racionalni z ustreznimi kontrolnimi postopki in lahko bistveno znižamo ogljični odtis.

## **1 INTRODUCTION**

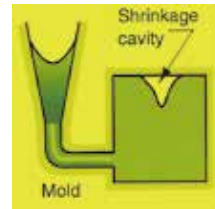
### **1.1 Basic or general defects of casting hidden mistakes for raw parts**

There are numerous opportunities for things to go wrong in terms of the quality of casting in the production of casting in foundries, thus resulting in quality defects in the product. These defects can be classified into two groups: general defects common to all casting processes, and defects related to the sand casting process. See Table 1 for examples of a casting that has solidified before completely filling a mould cavity, a casting in which two portions of metal flow together but there is a lack of fusion due to premature freezing, and a casting in which metal splatters during pouring and solid globules form and become trapped in the casting.

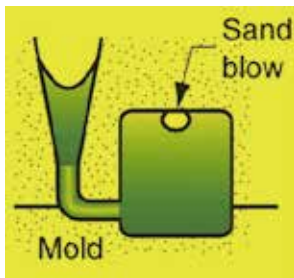
**Table 1: Basic casting defects [9]**



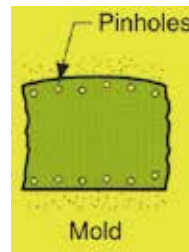
a) Metal splatters during pouring and solid globules form and become trapped in the casting.



a) A depression in a surface or internal void caused by solidification shrinkage that restricts the amount of molten metal available in the lowermost region from freezing.



a) A balloon-shaped gas cavity caused by the release of mould gases during pouring.



a) The formation of numerous small gas cavities at or slightly below the surface of the casting.

## 1.2 Control procedures for detection of hidden defects in the casting industry

The main purpose of non-destructive testing (NDT) is to examine the quality or conformity of inspected material with technical specification requirements and standards. Three inspection methods were used for the purposes of this paper: Visual testing (VT), Liquid penetrant testing (PT), Radiographic testing, i.e. x-ray – (RT).

### Visual inspection method

In a visual examination, it is possible to determine geometric and dimensional surface defects with the help of visible light and the human eye (and sometimes also devices).

### Liquid penetrant testing

The color penetrant, which fills the open defect to the surface due to its capillarity, enables extremely contrasting visibility of the defect when applied by the developer. Only surface defects can be detected.



**Figure 1: Liquid penetrant testing inspection method [10]**

### **Interpretation of Radiographic x-ray testing**

The most widely used non-destructive methods for detecting internal imperfections in cast products are radiographic and ultrasonic testing. The principles of how these methods work on different castings differ, and the basis for choosing one of the other depends on the type of casting, the type of casting material, the purpose of service, the undergoing load during service, the degree of safety and reliability, etc. The ultrasonic method (UT) is based on inducing the ultrasonic waves obtained in the transducer into material, whereby ultrasonic waves reflect from the eventual discontinuity (porosity, inclusions, shrinkage, cracks...) before returning. To obtain sound wave reflection, it is important that the shape of the imperfection with a major axis is approximately perpendicular to the sound beam axis. This means that the volumetric imperfections (porosity, inclusions) are well detected, regardless of the direction of the sound beam, however, planar flaws (cracks, some type of shrinkage, tears) can only be detected if the sound beam axis is approximately perpendicular to the major shallow flaw. These waves provide an indication on the ultrasonic instrument, so that the operator may conclude that there is an imperfection in the cast product. This allows the dimensional properties, and sometimes the origin, of particular imperfections in the casting volume to then be determined. Thereafter, an assessment can be made of whether or not the imperfections are acceptable based on pre-determined (as per specification) standardised acceptance criteria. The procedures for performing ultrasonic testing must follow standards, such as the EN 12680 series, various ASTMs and ASMEs. The standardised acceptance criteria are defined as various levels to permit more or less imperfections. The level of acceptance is usually selected based on the design requirements and service conditions. [10]

Radiographic testing (RT) is based on the attenuation of radiation energy while travelling through the material being tested. A radiation source (X-ray tube or gamma ray source) is required together with a detector to catch the differences in the radiation energy coming out of the material on

the opposite side. The larger the eventual imperfection in the material, the higher the detected level of energy intensity. Therefore, imperfections can be identified based on different densities of the film. The procedures for performing RT are standardised approaches, usually according to EN ISO 5579 or ASTM E94. These standards prescribe all the measures, parameters, equipment and settings to get a film image of a proper quality level in order to be ready for evaluation of any eventual imperfections. This includes the selection of proper sources (appropriate radiation energy), films, lead screens, based on material type and thickness, selection of appropriate distances from the source to the test object to achieve correct image sharpness, requirements for image quality indicators to prove that the image on film has achieved the required quality level, film density requirements, film processing requirements, etc. There is a slight difference between the requirements of EN ISO 5579 and ASTM E94 in terms of how they determine radiation energy selection, image quality indicator type and selection and determination of the sharpness [10].

Other standards related to RT are those for assessing and evaluating the imperfection of radiographic films following exposure and processing; these are ASTM E446, E186, E280 and E689. The listed ASTM standards provide rules/guidelines for evaluation of imperfection indications in castings detected on films. They also contain the reference radiographs at a 1:1 scale for comparison during the evaluation of the films. Evaluation of imperfections in cast products is based on a comparison between the actual film and the reference radiograph from the ASTMs. E446 relates to steel castings of a wall thickness up to 2" (51mm). There are three different volumes depending on the energy applied during exposure of the E446: Volume I: medium voltage (250kV x-ray), Volume II: 1MV x-ray or iridium-192 radiation, and Volume III: 2MV to 4MV rays and Cobalt-60 radiation. Reference radiographs of the correct volume must be selected while performing a particular evaluation based on the actual energy source used. Examples of a reference radiograph from ASTM E446 Volume I may be seen in the attached document (note: the document is not for official use). Similar radiographs are also included in ASTM E186, which covers castings with a wall thickness from 2" up to 4.5", and E280, which covers a wall thickness from 4.5" to 12". ASTM E689 is used for ductile iron castings (spheroidal graphite cast iron). This ASTM does not have specific reference radiographs but refers to the aforementioned reference radiographs for steel – ASTM E446, E186, E280. [10]

Whenever an evaluation is performed, e.g. according to E446, it is first necessary to recognise the type of defect; either it is porosity – Category A, or it is slag/sand inclusion – Category B, or it is shrinkage – Category C, etc. The second step is to determine the severity level for each particular category, if applicable. Level 1 is less severe whereas level 5 is the most severe – see Figure 2, Figure 3 and Figure 4, below.

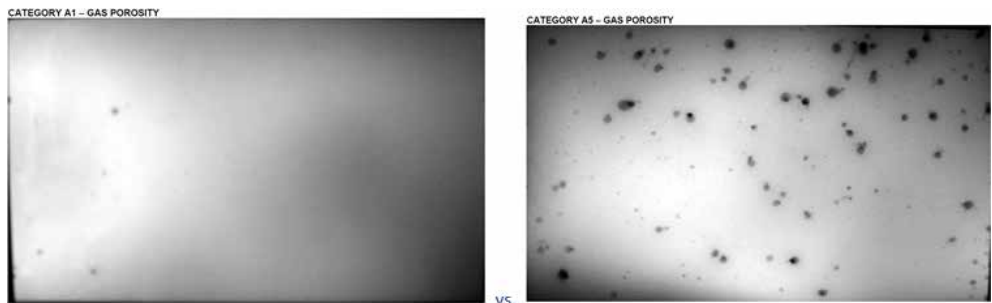


**Figure 2:** Interpretation of the results using x-ray inspection [10]

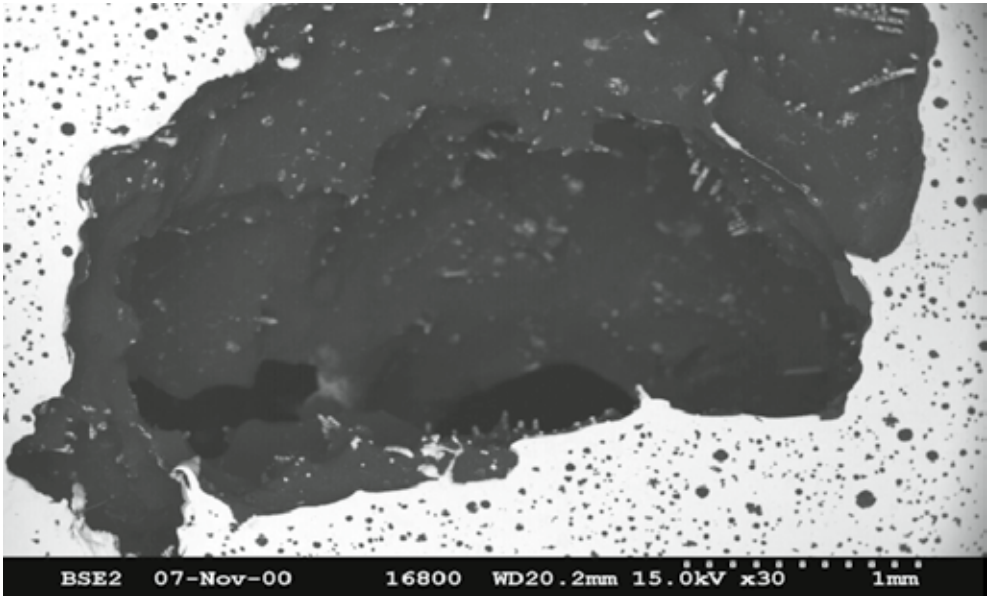


*Figure 3: Hydrogen gas porosity [9]*

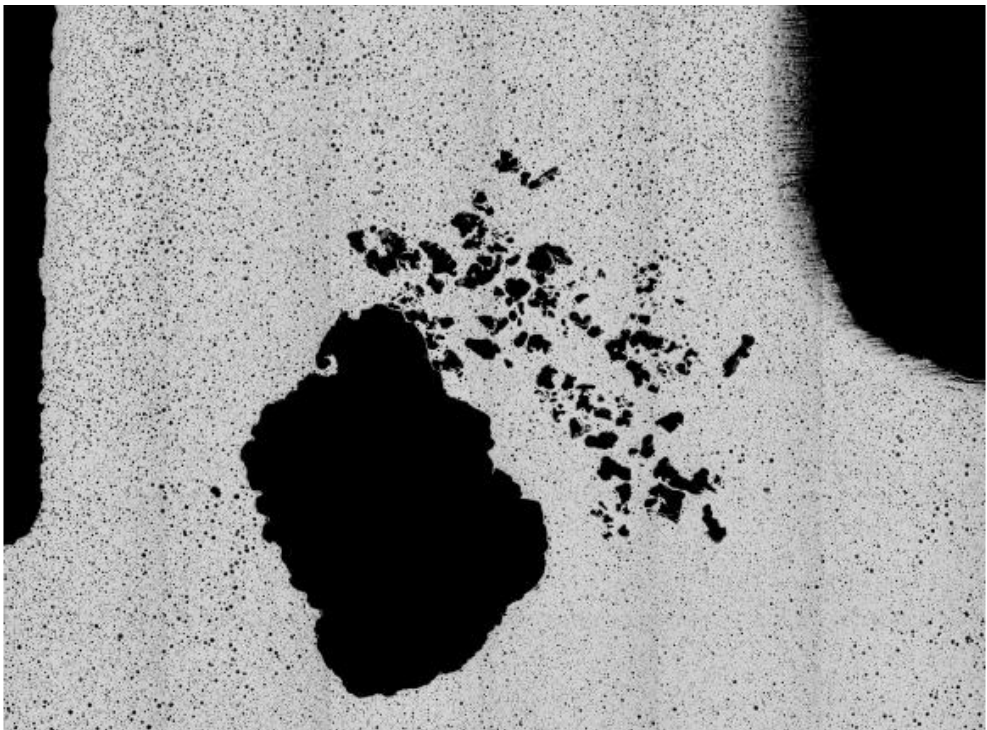


*Figure 4: Shrinkage porosity [9]*



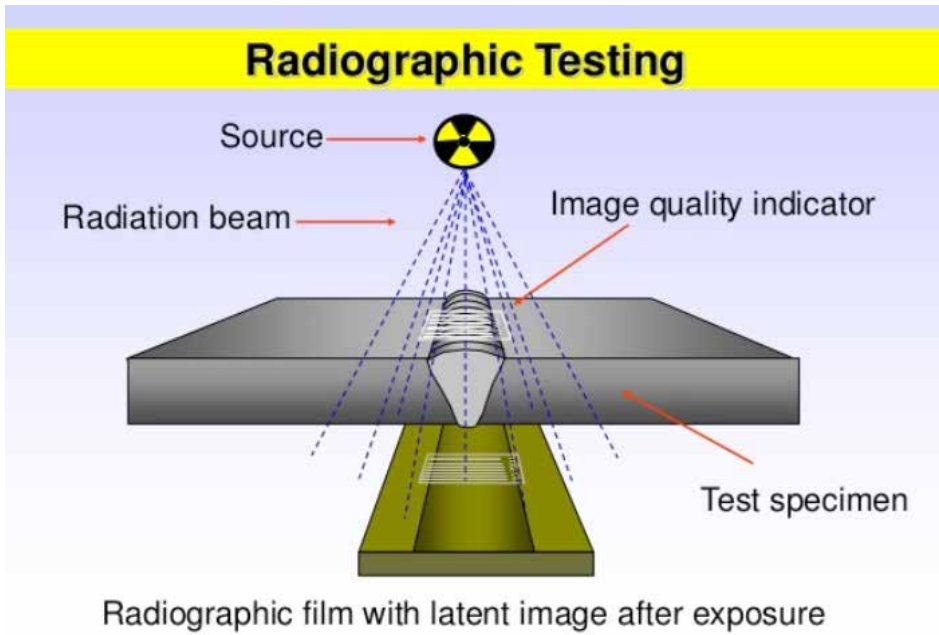


Figure 5: Schematic illustration of x-ray inspection method [1]

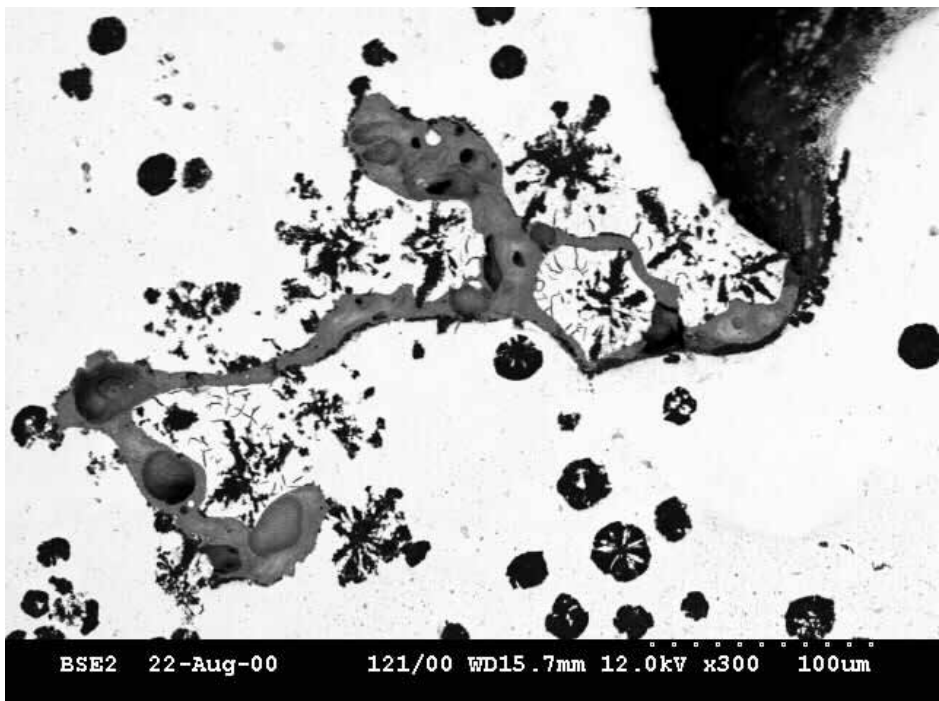


Figure 6: Slag inclusion defects [9]



**Figure 7:** Visible porosity on machined surface [9]

Slag inclusions resulted from incorrect discipline in the removal of slag from the ladle in foundry production, emptying of the ladle during procedures, improper improvements in the process of pouring and shaping of the casting system that reduce the use of filter or a slag trap, or a reduction in Mg content additives. Figure 6 shows an example of typical porosity or slag inclusions which are not allowed for critical components in the railway industry. There are high quality criteria for the safety component, which mean that this kind of component is present as scrap material.

## 2 EXPERIMENTAL PROCEDURE

The critical safety component of the brake holder was selected as the research subject for this paper. This is the most critical mechanical component in the railway industry, which was made at the casting production foundry in Ivančna Gorica for the final customer Knorr Bremse. The name of the product is KozolenBoltzen and it holds together the entire set of train brakes. The normal price of the product is around EUR 40 per raw part and EUR 25 for the machining price.

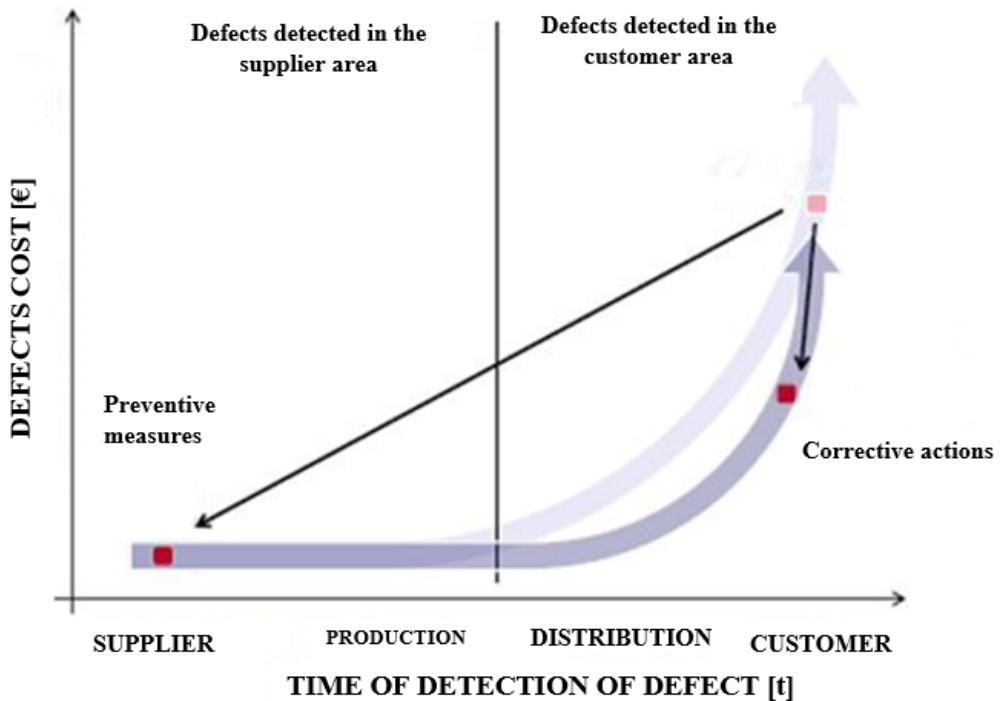


**Figure 8:** Management cost of defect in OEM supply chain [9]

For correct investigation of the basic example the sample must be captured in the correct way and at a precise interval. If the sample is too small, a realistic picture of the process cannot be obtained, and if the sample is too large it can lead to high costs. A large volume of samples provides information about irregularities in the process more quickly, however, this takes time. Data collection can take place for each product in the series and can be done once per shift or even once a day. However, it all depends on the importance of the characteristic. The sampling frequency of the sample data must also be specified. For the sampling frequency, it is necessary to determine whether the sampling will take place over a long time interval with more samples or over a short time interval with a smaller number of samples. As a rule, several small samples representing the whole population are taken in large batches.

There is a lot of low-hanging fruit ready to pick in most industrial sectors in terms of reducing energy consumption in manufacturing processes, such as newer and more efficient equipment, insulation on buildings, the use of LEDs, more effective logistics, etc. However, so much metal needs to be heated for the casting industry that this low-hanging fruit barely affects absolute energy consumption.

In addition, anyone can grab this low-hanging fruit, while addressing internal defects on casting is much harder than switching off a monitor left on standby, requiring years of engineering education in metallurgy, years of experience and a good brainstorming team.

The reduction of defective parts is the most effective measure to reduce energy consumption but also the most challenging to address. [5-8]

The Original Equipment Manufacturing (OEM) supply chain has changed dramatically since the 1970s, when automotive manufacturers and other large OEMs closed their own core processes and became massive outsourcing and offshoring labour-intensive casting and machining processes.

There were advantages to this new paradigm, as it allowed the optimisation of processes, the development of a new ecosystem of specialised supply chains and niche companies, a reduction in waste, faster R&D and lower costs.

There are, however, some downsides [5-7], particularly an increase in the carbon footprint of transporting parts and even worse, dealing with non-conformant products became a challenge. The machining site is no longer within minutes of the foundry, where casted parts with porosity could simply be recast and replaced by a new casting. There were no accounts of KPIs and PPMs in the middle of last century, only the memory of engineers who have since retired [4-5].

While since the 19<sup>th</sup> and 20<sup>th</sup> century foundries had been located in a building or were just minutes and metres away from the machining sites of shipyards, rail and later automotive facilities. Of late, however, offshoring means they have been moved further away – often days and hundreds or thousands of kilometres [3].

Dealing with rejects on casting has thus become a slow and time-consuming activity, ranging from being a nuisance to being problematic. One of the root causes of the increase in casting defects relates to the distance from design to casting, as ‘Design for Manufacturing’ needs good know-how and communication with the supplier, which is often not the case.

On the quality side, the ISO 9000 quality management standard was established in 1987 with guidelines intended to increase business efficiency and customer satisfaction. Due to the new requirement for quality assurance in the automotive sector, QS 9000 was established in 1992, led by Ford, General Motors and Chrysler in the US [8].

Other sectors followed the automotive trend of offshoring and requiring specific quality systems. The second wave was aerospace and in 1998, US aerospace contractors established AS 9000 based on ISO 9000. For the third wave, Europe created the International Rail Industry Standards (IRIS) in 2005 [1-3],[7].

These waves correlate with some major changes in the casting sector landscape. Increasing quality demands and a reduction in business volume hit the automotive sector. Many components were converted to other lighter materials and numerous foundries shut down due to higher volume and more efficient automation (horizontal) [2].

The reduction of time from concept to serial and increased product customisation presents another challenge for foundries by creating a ‘high mix, low volume’ of parts. Lower quantities of batches also challenge casting optimisation [2-3] as well as distant ‘Design for Manufacturing’, smaller batches and the technical challenges of detecting internal porosity. This becomes more necessary for critical safety components and difficult when even x-ray inspection is ineffective [1].

In recent years, many successful companies have been investing in reducing energy consumption and carbon footprint in all primary and secondary product manufacturing processes. Every step counts, since energy consumption can be drastically reduced by using proper planning process inspection methods in the casting industry [3-4].

Successful and leading corporations around the world are joining the EcoVadis tool programme, thanks to its unified and standardised networking and comparison and introduction of good practice across organisations. The EcoVadis methodology for assessing a company's sustainability management systems is based on international standards such as the Global Reporting Index (GRI), ISO 26000 and the guiding principles of the Global Compact [1],[6].

### 3 ANALYSIS OF RESULTS

#### 3.1 Alignment of a decrease defects on raw surfaces in the casting industry

The first thing to be aware of is that this is a critical safety part for trains, which means that defects are not permitted. Each foundry aims to produce products of the highest quality, however, there are always some defects, therefore it is necessary to create procedures for handling them correctly prior to sending them for X-ray inspection to ensure proper selection is made and additional money and capacity are not wasted on the supplier side. The most important process control in production is to decrease the scrap rate on raw surfaces.



Figure 9: 3D model of a KozolenBoltzen bracket pin sample part [9]

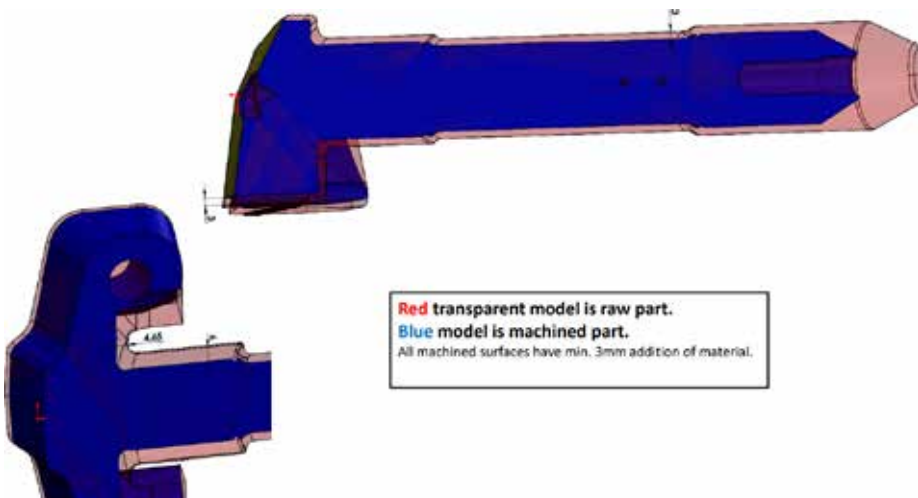


Figure 10: A cross section of a 3D model of a raw and machined part [9]

SCRATA surface comparators are used to classify the surface discontinuities for steel and iron castings. To date, the scrap discontinuities have been based on levels VC1 and VC2.

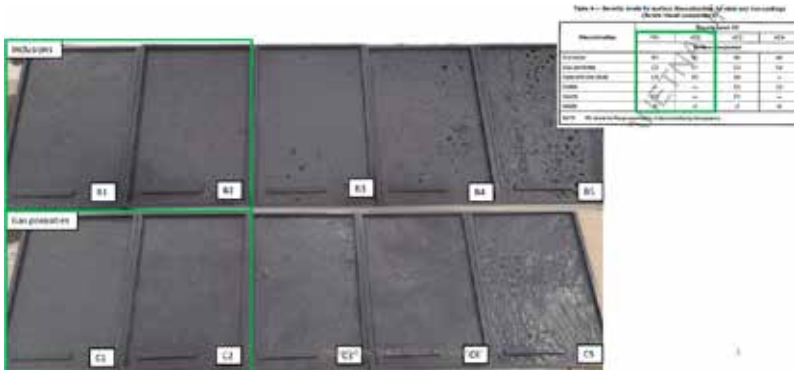


Figure 11: SCRATA plates Standard SIST EN 1370 [9].





Figure 12: Defects on machining surface [9]



Figure 13: Defects on the machining surface [9]

### 3.2 X-ray inspection detection of the hidden defect

Depth [mm]	Machined surface	Penetrated surface	Surface condition
4			without indications
5			without indications
5,5			without indications
6			without indications
6,5			without indications
7			without indications

**Figure 14:** Cutting inspection method using liquid penetrant P2 part with hidden defects [9]

Pictures below show where casting was sectioned. All sections were without indications.



**Figure 15:** Cutting P10 inspection method part [9]

## 4 CONCLUSIONS

To avoid defects in grey cast iron with spherical graphite it is necessary to:

- Use secondary raw materials that are of good quality and have low contents of accompanying elements (Mn, S, V, Mo, Ti, Cr...) and/or actively control the state of the melt.
- Have a stable melting and processing process of nodulation and grafting, resulting in repeatable analysis and good temperature efficiency.
- Use a high quality nodulator of an appropriate composition and granulation. Use quality vaccines that are specific to the requirements of the cast iron.

## References

- [1] Engineering choice. Available: <https://www.engineeringchoice.com/radiography-testing/> (31.03.2022)
- [2] **L. Magnusson Aberg, C. Hartung, J. Lacaze:** *Trace elements and the control limits in ductile iron*, 10th International Symposium on the Science and Processing of Cast Iron – SPCI10, Argentina, Mar del Plata, 2014
- [3] **J. Zhou:** *Colour Metallography of Cast Iron*, Spheroidal graphite Cast Iron–Part I, China Foundry, 2010
- [4] **] R. Elliott:** *Cast Iron Technology*, Butterworths, London, 1988
- [5] **V. Anjos:** *Use of Thermal Analysis to Control the Solidification Morphology of Nodular Cast Irons and Reduce Feeding Needs*, doktorska disertacija, Lisbon, Portugal, 2015
- [6] Ecovadis. Available: <https://support.ecovadis.com/hc/en-us/articles/115002653188-What-is-the-EcoVadis-assessment-process> (01.04.2022)
- [7] **S. F. Fischer, A. Bührig-Polaczek, J. Brachmann, P. Weiß:** *Influence of nickel and cobalt on microstructure of silicon solution strengthened ductile iron*, Materials Science and Technology, 31 Nemčija, 2015
- [8] **C. H. Hsu, M. L. Chen and C. J. Hu:** Microstructure and mechanical properties of 4% cobalt and nickel alloyed ductile irons, Materials Science and Engineering A 444
- [9] **T. Pavlin:** Internal investigation R&D dept. in melt area Livar d.d., 2021
- [10] American national standard EE446-98 reference radiographs for steel castings, USA, 2018



## Nomenclature

(Symbols)	(Symbol meaning)
<b><i>t</i></b>	Time
<b><i>X-ray</i></b>	Radiographic testing inspection
<b><i>GRI</i></b>	Global Reporting Index
<b><i>OEM</i></b>	Original equipment manufacturer
<b><i>VT</i></b>	Visual testing
<b><i>PT</i></b>	Liquid penetrant testing
<b><i>RT</i></b>	Radiographic testing
<b><i>NDT</i></b>	Non-destructive testing
<b><i>UT</i></b>	Ultrasonic method



# HAMILTONICITY OF CERTAIN CARTESIAN PRODUCTS OF GRAPHS

## HAMILTONSKOST KARTEZIČNEGA PRODUKTA GRAFOV

Tjaša Paj Erker<sup>1R</sup>

**Keywords:** Hamiltonicity, Cartesian product, path factor

### **Abstract**

A graph is Hamiltonian if it contains a spanning cycle. In this paper, we examine the hamiltonicity of the Cartesian product of a tree with a path. We offer sufficient conditions for the Cartesian product of a tree with a path to be Hamiltonian.

### **Povzetek**

Graf je Hamiltonov, če vsebuje cikel, ki gre skozi vsako vozlišče natanko enkrat. V tem članku preučujemo hamiltonskost kartezičnega produkta drevesa in poti. Podamo zadostne pogoje, da bo kartezični produkt drevesa in poti Hamiltonov.

## **1 INTRODUCTION**

A *Hamiltonian path* or *traceable path* is a path that visits each vertex of the graph exactly once. If there exists a Hamiltonian path in  $G$ , then  $G$  is referred to as *traceable*, and a graph is *Hamiltonian* if it contains a spanning cycle. In this article, we consider the hamiltonicity of the Cartesian product of two graphs. Our goal is to investigate the necessary and sufficient conditions for the Cartesian product to be Hamiltonian. We summarise some previous results and provide new ones. Certain results are related to those obtained in [2, 4].

<sup>R</sup> Corresponding author: Tjaša Paj Erker, University of Maribor, FME, Smetanova 17, 2000 Maribor, Slovenia. e-mail: tjasa.paj@um.si

<sup>1</sup> University of Maribor, FME, Smetanova 17, 2000 Maribor, Slovenia

Let  $G = (V(G), E(G))$  be a graph with vertex set  $V(G)$  and the edge set  $E(G)$ . The number of vertices in  $V(G)$  is the *order* of  $G$ . The degree of a vertex  $v$  is denoted by  $\deg G(v)$ . The maximum degree in  $G$  is denoted by  $\Delta(G)$ . The number of isolated vertices of  $G$  is denoted by  $i(G)$ . Let  $P_n$  denote a path of order  $n$  and  $C_n$  the cycle of order  $n$ . For convenience, we write  $V(P_n) = \{1, 2, \dots, n\}$  and  $E(P_n) = \{(i, i+1) \mid i = 1, 2, \dots, n-1\}$ . An *end-vertex* of  $G$  is a vertex of degree 1 in  $G$ . A *path factor* of a graph  $G$  is a spanning subgraph of  $G$  such that each component of the spanning subgraph is a nontrivial path. A graph has a  $\{P_2, P_3\}$ -factor if it has a spanning subgraph such that each component is isomorphic to  $P_2$  or  $P_3$ .

**Lemma 1.1** ([4]) *A graph  $G$  has a path factor if and only if  $G$  has a  $\{P_2, P_3\}$ -factor.*

If each component in a  $\{P_2, P_3\}$ -factor is isomorphic to  $P_2$ , the path factor is called *perfect matching*. The number of components of a graph  $G$  is denoted by  $c(G)$ . A graph  $G$  is  *$t$ -tough* ( $t \in \mathbb{R}$ ) if  $|S| > t \cdot c(G \setminus S)$  for every subset  $S \subseteq V(G)$  with  $c(G \setminus S) > 1$ .

Let  $G = (V(G), E(G))$  and  $H = (V(H), E(H))$  be graphs. The *Cartesian product* of  $G$  and  $H$  is the graph  $G \square H$  defined by  $V(G \square H) = V(G) \times V(H)$ , where  $(x_1, y_1)(x_2, y_2)$  is an edge in  $G \square H$  if  $x_1 = x_2$  and  $y_1 y_2 \in E(H)$ , or  $x_1 x_2 \in E(G)$ , and  $y_1 = y_2$ . The graphs  $G$  and  $H$  are termed *factors* of the product. For an  $x \in V(G)$ , the  *$H$ -layer*  $H_x$  is the set  $H_x = \{(x, y) \mid y \in V(H)\}$ .

## 2 CARTESIAN PRODUCT OF A TREE WITH A PATH

In this section we deal with Cartesian products of a tree with a path, i.e., we consider  $T \square P_n$ , for  $n \geq 4$  even.

**Proposition 2.1** ([3]) *Let  $G$  and  $H$  be both of odd order. If both  $G$  and  $H$  are bipartite, then  $G \square H$  is not Hamiltonian.*

Notice that when the order of  $T$  and  $n$  is both odd, the  $T \square P_n$  is not Hamiltonian by Proposition 2.1, so we will focus on even paths. The lemma below is from [1].

**Theorem 2.2** ([1]) *Let  $T$  be a tree with  $\Delta(T) \geq 2$  and  $C_n$  a cycle of order  $n$ . Then  $T \square C_n$  is Hamiltonian if and only if  $\Delta(T) \leq n$ .*

In [4], the authors showed that in the above theorem,  $T \square C_n$  cannot be replaced by  $T \square P_n$ . They give an example of a tree such that  $n = \Delta(T) + 1$  and  $T \square P_n$  is not Hamiltonian, proving that for a tree  $T_1$  with the vertex set  $V(T_1) = \{1, 2, 3, 4, 5, 6, 7, 8\}$  and the edge set  $E(T_1) = \{12, 23, 34, 45, 26, 37, 48\}$ , the graph  $T_1 \square P_4$  is not Hamiltonian.

From the figure below we can see that  $T_1 \square P_6$  is Hamiltonian. Therefore, we are interested in other examples of when this is possible.

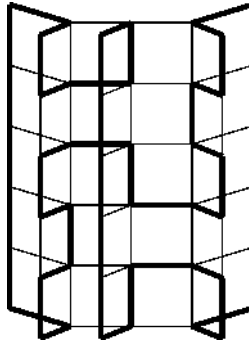


Figure 1: The Hamiltonian cycle in  $T_1 \square P_6$

In [4], the following result is proven.

**Proposition 2.3** ([4]) *Let  $H$  be a connected bipartite graph. Let  $n$  be an even integer and  $n \geq 4 \Delta(H) - 2$ . The following three statements are equivalent: (i)  $H \square P_n$  is Hamiltonian; (ii)  $H \square P_n$  is 1-tough; (iii)  $H$  has a path factor.*

Motivated by the example above (Figure 1), we will be interested in examples of such trees  $T$ , for which the condition  $n \geq 4 \Delta(H) - 2$  in proposition 2.3 is not fulfilled, yet  $T \square P_n$  is Hamiltonian.

**Proposition 2.4** ([4]) *Let  $T$  be a tree with perfect matching and  $n$  be a positive integer. The following three statements are equivalent: (i)  $T \square P_n$  is Hamiltonian; (ii)  $T \square P_n$  is 1-tough; (iii)  $n \geq \Delta(T)$ .*

Let  $T$  be a tree with  $\{P_2, P_3\}$ -factor  $F$ . We define the *type* of a vertex  $v$  with respect to  $F$  as follows:

- $v$  has type *EPL* if  $v$  is the left endpoint of a  $P_3$  in  $F$ ,
- $v$  has type *EPR* if  $v$  is the right endpoint of a  $P_3$  in  $F$ ,
- $v$  has type *M* if  $v$  is the middle vertex of a  $P_3$  in  $F$ ,
- $v$  has type *EP2* if  $v$  is a vertex of  $P_2$  in  $F$ .

**Theorem 2.5** *Suppose that  $T$  has a  $\{P_2, P_3\}$ -factor  $F$  and  $n$  is an even integer. If  $\deg_T(x) \leq (n+2)/2$  for every  $x$  of type *M* in  $F$ ,  $\deg_T(x) \leq n/2$  for every  $x$  of type *EP2* in  $F$  and  $\deg_T(x) + \deg_T(y) \leq (n+2)/2$  for every  $x, y$  of type *EPL* and *EPR* on every component in  $F$  isomorphic to  $P_3$ , then  $T \square P_n$  contains a Hamiltonian cycle.*

**Proof.** Let  $F$  be a  $\{P_2, P_3\}$ -factor which satisfies the conditions in the theorem. If each component in  $F$  is isomorphic to  $P_2$ , then  $T \square P_n$  by proposition 2.4 contains a Hamiltonian cycle, since every vertex  $x$  in  $T$  has type *EP2* and therefore  $\deg_T(x) \leq \Delta(T) \leq n/2 \leq n$ .

So, we can assume that there exist a component isomorphic to  $P_3$ .

First, we define the standard Hamiltonian cycle for  $P_3 \square P_n$  and for  $P_2 \square P_n$ .

For  $\{x, y, z\} \in V(P_3)$ ,  $\{xy, yz\} \in E(P_3)$  and an even  $n$ , we define the set  $\{(x, 1)(y, 1)\} \cup \{(y, 2i-1)(z, 2i-1), (z, 2i-1)(z, 2i), (z, 2i)(y, 2i) \mid 1 \leq i \leq n/2\} \cup \{(y, 2i)(y, 2i+1) \mid 1 \leq i \leq (n-2)/2\} \cup \{(y, n)(x, n)\} \cup \{(x, i)(x, i+1) \mid 1 \leq i < n\}$  of edges in  $P_3 \square P_n$  as the standard Hamiltonian cycle for  $P_3 \square P_n$  (see Figure 2 (left)).

For  $\{u, v\} \in V(P_2)$ , we define the set  $\{(u, 1)(v, 1)\} \cup \{(v, i)(v, i+1) \mid 1 \leq i \leq n\} \cup \{(u, i)(u, i+1) \mid 1 \leq i < n\} \cup \{(u, n)(v, n)\}$  of edges in  $P_2 \square P_n$  as the standard Hamiltonian cycle for  $P_2 \square P_n$  (see Figure 2 (right)).

Notice that there are  $(n-2)/2$  vertical edges on every  $P_n$ -layer that correspond to a vertex  $y \in F$  of type  $M$  on the standard Hamiltonian cycle  $P3 \square Pn$  and that there are  $n/2$  vertical edges on every  $P_n$ -layer that correspond to a vertex  $y \in F$  of type  $EPR$  on the standard Hamiltonian cycle  $P3 \square Pn$ .

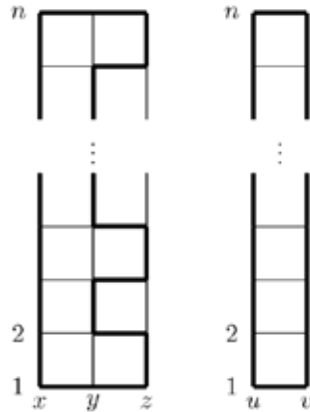


**Figure 2:** The standard Hamiltonian cycle for  $P3 \square Pn$  and for  $P2 \square Pn$

We now use a recursive construction to reach a Hamiltonian cycle in  $T \square Pn$ . We start with the standard Hamiltonian cycle for  $C' = C1 \square Pn$  of initially chosen component  $C_1$  in  $F$ . Let  $C_2$  be a component in  $F$  such that there is a vertex  $y \in C_2$  adjacent with a vertex  $x \in C_1$  (note that  $xy \in E(T)$ ) and let  $C'' = C2 \square Pn$  be a standard Hamiltonian cycle as described above. We can join such two standard cycles  $C'$  and  $C''$  with cycle  $C'''$  with vertex set  $V(C''') = V(C') \cup V(C'')$  and edge set  $E(C''')$  as described below.

We distinguish several cases:

- (i)  $C_1$  and  $C_2$  are isomorphic to  $P_2$

We can join cycles  $C'$  and  $C''$  with cycle  $C'''$  with edge set  $E(C''') = ((E(C') \cup E(C'')) \setminus \{(x, i)(x, i+1), (y, i)(y, i+1)\}) \cup \{(x, i)(y, i), (x, i+1)(y, i+1)\}$  for every  $i = 1, 2, \dots, n-1$  (see Figure 3 (a)).

- (ii)  $C_1$  is isomorphic to  $P_2$  and  $C_2$  is isomorphic to  $P_3$  (or vice-versa).

If  $y$  has type  $M$ , we can join such cycles  $C'$  and  $C''$  with cycle  $C'''$  with edge set  $E(C''') = ((E(C') \cup E(C'')) \setminus \{(x, 2i)(x, 2i+1), (y, 2i)(y, 2i+1)\}) \cup \{(x, 2i)(y, 2i), (x, 2i+1)(y, 2i+1)\}$  for every  $i = 1, 2, \dots, (n-2)/2$  (see Figure 3 (b)).

If  $y$  has type  $EPR$  (or  $EPL$ ), we can join cycles  $C'$  and  $C''$  with cycle  $C'''$  with edge set  $E(C''') = ((E(C') \cup E(C'')) \setminus \{(x, 2i-1)(x, 2i), (y, 2i-1)(y, 2i)\}) \cup \{(x, 2i-1)(y, 2i-1), (x, 2i)(y, 2i)\}$  for every  $i = 1, 2, \dots, n/2$  (see Figure 3 (c)).

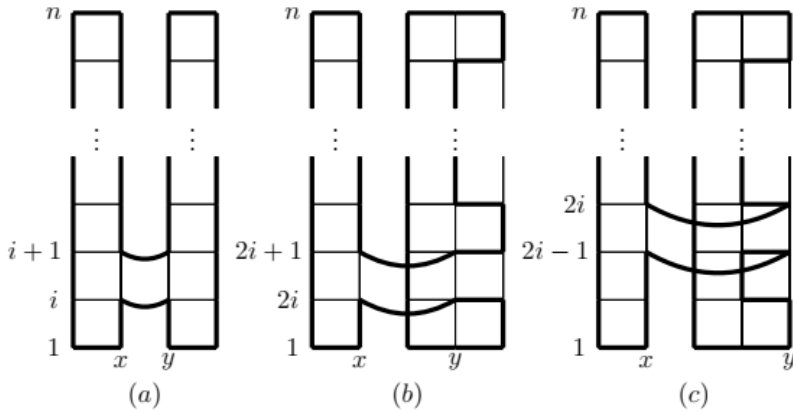


**Figure 3:** Joining standard cycles  $C'=C1 \square P_n$  and  $C''=C2 \square P_n$  for  $P2 \square P_n$  where  $C1$  is isomorphic to  $P2$

(iii)  $C_1$  and  $C_2$  are isomorphic to  $P_3$ .

If  $x$  and  $y$  have type  $M$ , we can join cycles  $C'$  and  $C''$  with cycle  $C'''$  with edge set  $E(C''') = ((E(C') \cup E(C'')) \setminus \{(x, 2i)(x, 2i + 1), (y, 2i)(y, 2i + 1)\}) \cup \{(x, 2i)(y, 2i), (x, 2i + 1)(y, 2i + 1)\}$  for every  $i = 1, 2, \dots, (n-2)/2$  (see Figure 4 (a)).

If  $x$  and  $y$  have type  $EPR$  (or  $EPL$ ), we can join cycles  $C'$  and  $C''$  with cycle  $C'''$  with edge set  $E(C''') = ((E(C') \cup E(C'')) \setminus \{(x, 2i-1)(x, 2i), (y, 2i-1)(y, 2i)\}) \cup \{(x, 2i-1)(y, 2i-1), (x, 2i)(y, 2i)\}$  for every  $i = 1, 2, \dots, n/2$  (see Figure 4 (b)).

If  $x$  has type  $M$  and  $y$  has type  $EPL$ , we can join such two standard cycles  $C'$  and  $C''$  with cycle  $C'''$  with edge set  $((E(C') \cup E(C'')) \setminus \{(x, 2i)(x, 2i + 1), (y, 2i)(y, 2i+1)\}) \cup \{(x, 2i)(y, 2i), (x, 2i+1)(y, 2i+1)\}$  for every  $i = 1, 2, \dots, (n-2)/2$  (see Figure 4 (c)).

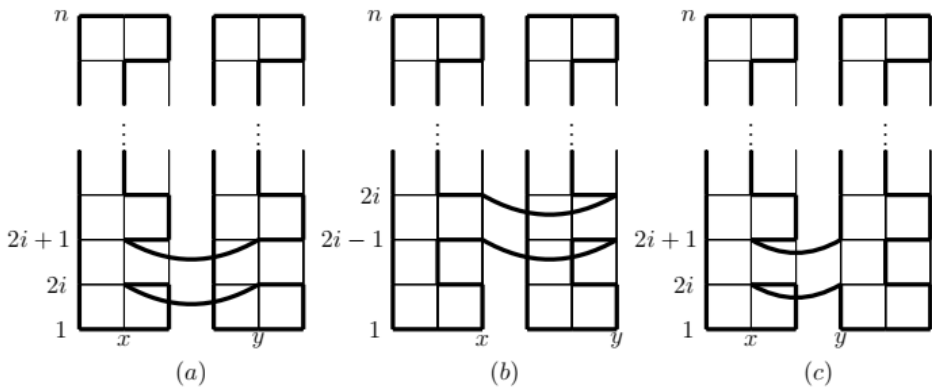


**Figure 4:** Joining standard cycles  $C'=C1 \square P_n$  and  $C''=C2 \square P_n$  for  $P2 \square P_n$  where  $C1$  is isomorphic to  $P3$

If  $x$  has type  $M$  and  $y$  has type  $EPR$ , we reshape the standard Hamiltonian cycle  $C''=P_3 \square P_n$  into  $C^R$ . Denote  $y = y_3$  and  $\{y_1, y_2, y_3\} \in V(P_3)$  where  $\{y_1 y_2, y_2 y_3\} \in E(P_3)$ . Define,  $C^R = (C' \setminus \{(y_1, 2i)(y_1, 2i+1), (y_2, 2i)(y_3, 2i), (y_2, 2i+1)(y_3, 2i + 1)\}) \cup \{(y_1, 2i)(y_2, 2i), (y_1, 2i + 1)(y_2, 2i + 1), (y_3, 2i)(y_3, 2i + 1)\}$  for some

$i = 1, 2, \dots, (n-2)/2$  (see Figure 5 (a)). Now we can join two of such cycles  $C^i$  and  $C^R$  with cycle  $C''$  with edge set  $((E(C^i) \cup E(C^R)) \setminus \{(x, 2i)(x, 2i + 1), (y_3, 2i)(y_3, 2i + 1)\}) \cup \{(x, 2i)(y_3, 2i), (x, 2i+1)(y_3, 2i+1)\}$  (see Figure 5 (b)).

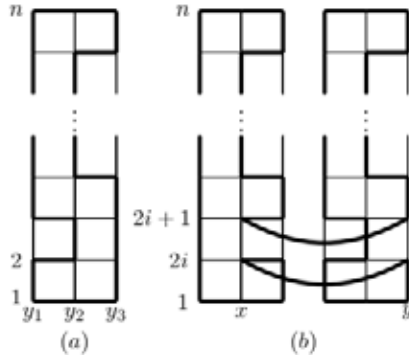


**Figure 5:** The redesigned standard Hamiltonian cycle  $CR$  for  $P_3 \square P_n$  (a) and joining standard cycles  $C' = P_3 \square P_n$  and  $CR$  (b)

For  $t = 2, 3, \dots$  we repeat the following until we reach a Hamiltonian cycle for  $T \square P_n$ . Let  $C_t$  be a component of  $T \setminus C_{t-1}$  such that there is a vertex  $x \in C_t$  incident with the vertex on  $C_{t-1}$ . We join standard Hamiltonian cycle  $C_t \square P_n$  with the cycle  $C_{t-1} \square P_n$  as described above. The construction is correct since it consists of the repeated joining of cycles at incident vertices in  $T$ , and there are enough free edges to join all standard Hamiltonian cycles, namely:

- for every  $x \in C_{t-1}$  of type  $EP_2$ , we have at most  $deg_T(x) - 1 \leq n/2 - 1 = (n-2)/2$  component  $C_j$  adjacent with  $x$ , so there are enough free vertical edges on  $P_n$ -layer  $P_{nx}$  to join cycle  $C' = C_{t-1} \square P_n$  with all cycles  $C'' = C_j \square P_n$  as described above;
- for every  $x \in C_{t-1}$  of type  $M$ , we have at most  $deg_T(x) - 2 \leq (n+2)/2 - 2 = (n-2)/2$  component  $C_j$  adjacent with  $x$ , so there are enough free vertical edges on  $P_n$ -layer  $P_{nx}$  to join cycle  $C' = C_{t-1} \square P_n$  with all cycles  $C'' = C_j \square P_n$  as described above;
- for every  $x, y \in C_{t-1}$  of type  $EPL$  and  $EPR$ , we have at most  $deg_T(x) + deg_T(y) - 2 \leq (n+2)/2 - 2 = (n-2)/2$  component  $C_j$  adjacent with  $x$  and  $y$ , so there are enough free vertical edges on  $P_n$ -layer  $P_{nx}$  or  $P_{ny}$  to join cycle  $C' = C_{t-1} \square P_n$  with all cycles  $C'' = C_j \square P_n$  as described above.  $\square$

## References

- [1] **V. Batagelj, T. Pisanski:** *Hamiltonian cycle in the cartesian product of a tree and a cycle*, Discrete Math. 38, 311 – 312, 1982
- [2] **R. Čada, E. Flandrin, H. Li:** *Hamiltonicity and pancyclicity of cartesian products of graphs*, Discrete Math. 309, 6337 – 6343, 1987
- [3] **V. Dimakopoulos, L. Palios, A. S. Poulakidas:** *On the Hamiltonicity of the Cartesian product*, Inform. Process. Lett. 96, 49 – 53, 2005
- [4] **L. Kao, C. Weng:** *The Relation Between Hamiltonian and 1-Tough Properties of the Cartesian Product Graphs*, Graphs Comb., 2020
- [5] **M. Rosenfeld, D. Barnette:** *Hamiltonian circuits in certain prisms*, Discrete Math. 5, 389394, 1973





# MAIN TITLE OF THE PAPER SLOVENIAN TITLE

*Author<sup>1</sup>, Author<sup>2</sup>, Corresponding author<sup>✉</sup>*

Keywords: (Up to 10 keywords)

## **Abstract**

Abstract should be up to 500 words long, with no pictures, photos, equations, tables, only text.

## **Povzetek**

(Abstract in Slovenian language)

**Submission of Manuscripts:** All manuscripts must be submitted in English by e-mail to the editorial office at [jet@um.si](mailto:jet@um.si) to ensure fast processing. Instructions for authors are also available online at <http://www.fe.um.si/en/jet/author-instructions.html>.

**Preparation of manuscripts:** Manuscripts must be typed in English in prescribed journal form (MS Word editor). A MS Word template is available at the Journal Home page.

A title page consists of the main title in the English and Slovenian language; the author(s) name(s) as well as the address, affiliation, E-mail address, telephone and fax numbers of author(s). Corresponding author must be indicated.

**Main title:** should be centred and written with capital letters (ARIAL bold 18 pt), in first paragraph in English language, in second paragraph in Slovenian language.

**Key words:** A list of 3 up to 6 key words is essential for indexing purposes. (CALIBRI 10pt)

**Abstract:** Abstract should be up to 500 words long, with no pictures, photos, equations, tables, - text only.

**Povzetek:** - Abstract in Slovenian language.

**Main text** should be structured logically in chapters, sections and sub-sections. Type of letters is Calibri, 10pt, full justified.

---

✉ Corresponding author: Title, Name and Surname, Organisation, Department, Address, Tel.: +XXX x xxx xxx, E-mail address: x.x@xxx.xx

<sup>1</sup> Organisation, Department, Address

<sup>2</sup> Organisation, Department, Address

Units and abbreviations: Required are SI units. Abbreviations must be given in text when first mentioned.

Proofreading: The proof will be send by e-mail to the corresponding author in MS Word's Track changes function. Corresponding author is required to make their proof corrections with accepting or rejecting the tracked changes in document and answer all open comments of proof reader. The corresponding author is responsible to introduce corrections of data in the paper. The Editors are not responsible for damage or loss of submitted text. Contributors are advised to keep copies of their texts, illustrations and all other materials.

The statements, opinions and data contained in this publication are solely those of the individual authors and not of the publisher and the Editors. Neither the publisher nor the Editors can accept any legal responsibility for errors that could appear during the process.

Copyright: Submissions of a publication article implies transfer of the copyright from the author(s) to the publisher upon acceptance of the paper. Accepted papers become the permanent property of "Journal of Energy Technology". All articles published in this journal are protected by copyright, which covers the exclusive rights to reproduce and distribute the article as well as all translation rights. No material can be published without written permission of the publisher.

Chapter examples:

## 1 MAIN CHAPTER

**(Arial bold, 12pt, after paragraph 6pt space)**

### 1.1 Section

**(Arial bold, 11pt, after paragraph 6pt space)**

#### 1.1.1 Sub-section

**(Arial bold, 10pt, after paragraph 6pt space)**

Example of Equation (lined 2 cm from left margin, equation number in normal brackets (section. equation number), lined right margin, paragraph space 6pt before in after line):

$$\text{Equation} \tag{1.1}$$

Tables should have a legend that includes the title of the table at the top of the table. Each table should be cited in the text.

Table legend example:

***Table 1: Name of the table (centred, on top of the table)***

Figures and images should be labelled sequentially numbered (Arabic numbers) and cited in the text – Fig.1 or Figure 1. The legend should be below the image, picture, photo or drawing.

Figure legend example:

**Figure 1:** *Name of the figure (centred, on bottom of figure, photo, or drawing)*

## References

- [1] **N. Surname:** *Title*, Journal Title, Vol., Iss., p.p., Year of Publication
- [2] **N. Surname:** *Title*, Publisher, Year of Publication
- [3] **N. Surname:** *Title* [online], Publisher or Journal Title, Vol., Iss., p.p., Year of Publication. Available: website (date accessed)

Examples:

- [1] **J. Usenik:** *Mathematical model of the power supply system control*, Journal of Energy Technology, Vol. 2, Iss. 3, p.p. 29 – 46, 2009
- [2] **J. J. DiStefano, A.R. Stubberud, I. J. Williams:** *Theory and Problems of Feedback and Control Systems*, McGraw-Hill Book Company, 1987
- [3] **T. Žagar, L. Kegel:** *Preparation of National programme for SF and RW management taking into account the possible future evolution of ERDO* [online], Journal of Energy Technology, Vol. 9, Iss. 1, p.p. 39 – 50, 2016. Available: [http://www.fe.um.si/images/jet/Volume\\_9\\_Issue1/03-JET\\_marec\\_2016-PREPARATION\\_OF\\_NATIONAL.pdf](http://www.fe.um.si/images/jet/Volume_9_Issue1/03-JET_marec_2016-PREPARATION_OF_NATIONAL.pdf) (7. 10. 2016)

Example of reference-1 citation: In text [1], text continue.

## Nomenclature

(Symbols)	(Symbol meaning)
t	time



ISSN 1855-5748



9 771855 574008